OLD DOMINION UNIVERSITY RESEARCH FOUNDATION

DEPARTMENT OF MATHEMATICAL AND COMPUTING SCIENCES
SCHOOL OF SCIENCES AND HEALTH PROFESSIONS
OLD DOMINION UNIVERSITY
NORFOLK, VIRGINIA

LONG-TERM TEMPERATURE EFFECTS ON GaAs SOLAR CELLS

By

John H. Heinbockel

and

Ki H. Hong

Final Report
For the period January 1, 1978 - April 15, 1979

Prepared for the
National Aeronautics and Space Administration
Langley Research Center
Hampton, Virginia

Under
Research Grant NSG 1465
Edmund J. Conway, Technical Monitor
Space Systems Division

April 1979

DEPARTMENT OF MATHEMATICAL AND COMPUTING SCIENCES
SCHOOL OF SCIENCES AND HEALTH PROFESSIONS
OLD DOMINION UNIVERSITY
NORFOLK, VIRGINIA

LONG-TERM TEMPERATURE EFFECTS ON GaAs SOLAR CELLS

By

John H. Heinbocke

and

Ki H. Hong

Final Report
For the period January 1, 1978 - April 15, 1979

Prepared for the
National Aeronautics and Space Administration
Langley Research Center
Hampton, Virginia 23665

Under
Research Grant NSG 1465
Edmund J. Conway, Technical Monitor
Space Systems Division

Submitted by the
Old Dominion University Research Foundation
P.O. Box 6369
Norfolk, Virginia 23508

April 1979

TABLE OF CONTENTS

LIST OF TABLES

LIST OF FIGURES

ACKNOWLEDGMENTS

The authors would like to thank E. Conway, G. Walker, and C. Byvik of NASA/Langley Research Center for their comments and discussions during the course of this study. We would also like to thank A. Tennille, J. Nodurft, and M. Lippman of the Old Dominion University Research Foundation for their help in the preparation of this report.

LONG-TERM TEMPERATURE EFFECTS ON GaAs SOLAR CELLS

By

John H. Heinbockel[1] and Ki H. Hong[2]

SUMMARY

The thermal degradation of AlGaAs-GaAs solar cells resulting from a long-term operation in a space environment is investigated. The solar cell degradation effects caused by zinc and aluminum diffusion as well as deterioration by arsenic evaporation are presented.

Also in this report, we present the results of experimental testing and measurements of various GaAs solar cell properties while the solar cell was operating in the temperature range of 27° C to 350° C. In particular, the properties of light current voltage curves, dark current voltage curves, and spectral response characteristics are presented.

Finally, some theoretical models for the annealing of radiation damage over various times and temperatures are presented.

INTRODUCTION AND STATEMENT OF PROBLEM

It is the purpose of this report to obtain fundamental information on the long-term effects of high operating temperatures on GaAs solar cell characteristics. Research was conducted in order to identify and obtain limits for the magnitudes of probable high-temperature effects on the GaAs solar cell characteristics.

In order to summarize the thermal degradation effects on GaAs solar cells: (1) a literature survey was performed, (2) basic laboratory experiments were performed to obtain the necessary fundamental information that

---

[1] Professor, Department of Mathematical and Computing Sciences, Old Dominion University, Norfolk, Virginia 23508.

[2] Research Professor, Department of Mathematical and Computing Sciences, Old Dominion University, Norfolk, Virginia 23508.

will be needed for the design and usage of GaAs solar cells in a space environment over a 10-year time period, and (3) theoretical models were developed in order to estimate the removal of radiation damage effects due to annealing at high temperatures.

Discussion is divided into three parts concerned with (1) thermal degradation of AlGaAs-GaAs solar cells due to zinc and aluminum diffusion, (2) experimental results of testing AlGaAs-GaAs solar cells at high temperatures (27° to 350° C), and (3) development of theoretical models for the prediction of annealing effects on the removal of radiation damage experienced by GaAs solar cells operating in a space environment.

LIST OF SYMBOLS

ΔX_j	change in junction depth
D_{Al}, D_{Zn}	thermal diffusion coefficients
J_{sc}	current density
V	voltage
V_{oc}	open circuit voltage
FF	fill factor
η	efficiency
q	electron charge
K	Boltzmann constant
A	factor
J_o	saturation current densit
n_i	intrinsic carrier density
W	width of depletion region
τ_c	composite lifetime
D	diffusion coefficients
τ	lifetime
E_a	activation energy

ω_o	jump frequency for interstitials
I_{sc}	short circuit current
T_m	energy transferred to lattice atoms (eV
E_e	electron energy
m_e	electron mass
c	velocity of light
M	lattice atom mass
E_d	displacement threshold energy
N	total number of defects/cm^3
σ_d	displacement cross section (cm^2)
N_ℓ	number of lattice atoms
Φ	1-MeV electron fluence (e/cm^2)
V_n	vacancies
i_n	interstitials
K_j	reaction rates
t	time
N_r	defects remaining after annealing
Φ_e	equivalent fluence
τ	annealing time
L, L_o	diffusion lengths
S_g, S_{go}	surface recombination velocities
K_g, K_s	damage coefficients
$\tilde{\phi}$	irradiation rate
T	temperature
T_o, T_a	temperatures

THERMAL DEGRADATION OF AlGaAs-GaAs SOLAR CELLS

Recently many reports on radiation damage of AlGaAs-GaAs solar cells in a simulated space environment have appeared (refs. 1 to 3). We are concerned about the thermal degradation of GaAs solar cells over a 10-year period of operation in a space environment. During this project, we studied the thermal deterioration of AlGaAs-GaAs solar cells which could result from a long-term operation in space. In order to assess the potential severity of the solar cell degradation, we assumed that the solar cell operated at a temperature of either 250° C or 350° C and in high vacuum conditions, i.e., 10^{-10} to 10^{-11} torr.

The AlGaAs-GaAs solar cell has a three-layer structure. The bottom layer is nGaAs which is 200 to 350-μm thick. The middle layer contains zinc doped pGaAs and is approximately 1-μm thick. The top layer is a conducting layer of pAlGaAs grown by the liquid phase epitaxy (LPE) method and doped with zinc and is less than 1-μm thick.

We investigated three potential mechanisms which may cause the solar cell to permanently deteriorate. These are (1) zinc diffusion for the Zn-doped p-layer into nGaAs, (2) aluminum diffusion from the LPE grown layer into the substrate, and (3) arsenic evaporation. For this study we employed currently available empirical data to predict potential deterioration. For the Zn diffusion we assumed that the total thickness of the Zn-doped p-layer is about 1 μm. Zinc diffusion during operation at temperatures in the range of 250° to 350° C for a period of 10 years was expected to increase the junction depth. There are many reports on Zn diffusion into GaAs (refs. 4 to 6). In this study we selected two different Zn diffusion coefficients. These diffusion coefficients were obtained from curve fitting of data from both elemental (ref. 4) and ternary sources (ref. 5). One diffusion coefficient was for temperatures below 800° C and the other was for temperatures below 744° C. Both data curves were extrapolated to 350° C and 250° C in order to estimate the junction depth change ΔX_j, which was assumed to be the distance from a step function gradient in the zinc concentration. The resulting junction depth changes, which are given in table 1, agree within 30 percent of each other. We believe that this 30 percent difference results from the experimental error or the

inaccurate determination of the diffusion coefficients during the curve fitting. The changes depicted in table 1, of approximately 0.1 μm, are small compared with the total p-layer thickness. However, this change of 0.1 μm could be important for radiation resistance cells having junction depths less than 0.5 μm.

Table 1. Thermal degradation of AlGaAs-GaAs solar cell for 10 years of operation.

Temperature (°C)	Change in Junction Depth ΔX_j (μm)		Arsenic Evaporation (mg)	
			GaAs	Zn-GaAs
250	$6.98(10^{-4})$[a]	$8.81(10^{-4})$[b]		
350	$5.78(10^{-2})$[a]	$9.9(10^{-2})$[b]	$4.45(10^{-9})$[c]	$6.76(10^{-7})$[c]
			No arsenic left[d]	

[a]Reference 4. [b]Reference 5. [c]Reference 8. [d]Reference 9.

For aluminum diffusion there is the problem of the movement of the GaAlAs-GaAs interface. We assume that the top layer of an AlGaAs-GaAs solar cell is composed of (Al_yGa_{1-y}) with y = 0.9. Chang and Koma (ref. 7) have recently studied interdiffusion of Al and Ga in $(Al_yGa_{1-y})As$ as a function of temperature and aluminum composition. The aluminum diffusion coefficient and activation energy in GaAs can be compared with the zinc diffusion coefficient in GaAs. The thermal diffusion coefficient (D_{Al}) of aluminum in GaAs at 350° C is approximately $1.7(10^{-31})$ cm^2/sec, whereas the thermal diffusion coefficient of zinc (D_{Zn}) in GaAs is approximately 10^{-20} cm^2/sec. The activation energies for diffusion of Al, Ga, and Zn in GaAs are 3.6 eV, 4.2 eV, and 2.49 eV, respectively. The aluminum diffusion coefficient is approximately 10^{-11} smaller than the zinc diffusion coefficient; therefore, a junction depth change due to aluminum diffusion can be ignored.

Arsenic evaporation can occur when an AlGaAs-GaAs solar cell is operated at high temperatures. This is because arsenic vapor evaporates from the surface of the solar cell at high temperatures, and this decomposes the GaAs. The arsenic loss from a GaAs surface creates crystal defects, and these defects form recombination centers and alter the composition of the GaAs surface structure. The arsenic contained in a 1-cm^2, 1-μm thick GaAs layer is approximately 0.7 mg. Based on recent kinetic studies, we can calculate total arsenic loss for AlGaAs-GaAs solar cell when the solar cell operates at 350° C in space for 10 years. Using the results of Lou et al. (ref. 8), we estimate the total arsenic loss to be approximately 6.7×10^{-7} mg over 10 years. Accordingly the density of arsenic vacancy is approximately 5×10^{16}/cc. This density is a factor of 10^2 lower than the dopant density in the p-layer, and hence the total arsenic loss is negligible and a surface stoichiometry is maintained. On the other hand, total arsenic loss based on Arthur's results (ref. 9) suggests a more serious problem. The estimated arsenic loss rate from the GaAs surface is 1.25×10^{-7} mg/cm^2-sec, which implies that all arsenic in a 1-μm layer of GaAs could evaporate within 2.5 months. Recently Sebestyen et al. (ref. 10) reported the arsenic loss from metal-covered GaAs. The calculated arsenic loss based on these experimental arsenic evaporation rates is shown in table 1. Based on the results of Lou et al. and Sebestyen et al. (refs. 8 to 10), it is difficult to have confidence in any estimate of arsenic evaporation rates.

As a direct observation of solar cell deterioration, we heated an AlGaAs-GaAs solar cell to approximately 300° C in a gas-tight enclosure with a quartz window for approximately 100 hours. From our direct observation of photovoltaic parameters, there was no significant degradation in the solar cell characteristics due to short-term exposure to high temperature. Consequently, we feel that further work is needed on the problem of arsenic evaporation in order to quantitatively predict long-term arsenic loss (surface defects on GaAs and composition change) at high temperature.

THERMAL PROPERTIES OF AlGaAs-pGaAs-nGaAs SOLAR CELLS

Introduction

Gallium arsenide (GaAs) solar cells are being considered for use in generating electrical power in space on a solar power satellite. They are also being considered for use in a high-temperature, near-Sun space science mission. The space environment in which the solar cells will be operating will have high temperatures and high doses of radiation which, over long periods of time, degrade the operation of conventional solar cells. Gallium arsenide solar cells have certain advantages over conventional solar cells. These advantages are (1) a higher band gap, (2) higher open circuit voltage, (3) capability of operating at a higher temperature, (4) a high resistance to radiation, and (5) a spectral response which more closely matches the Sun's solar spectrum.

In the sections that follow we will be concerned with the operational characteristics of pAlGaAs-pGaAs-nGaAs solar cells operating within the temperature range of 27° C to 350° C. Test data was obtained from GaAs solar cells operating in a simulated space environment. This test data characterizes the photovoltaic parameters which, as functions of temperature, determine the behavior of GaAs solar cells.

The test data, recorded as functions of temperature, consisted of illuminated current voltage curves, dark current voltage curves, and spectral response curves.

Experimental Considerations

The following describes the experimental work that was performed in order to determine the high-temperature GaAs solar cell thermal properties. Ten heteroface pGaAlAs/pGaAs/nGaAs solar cells were fabricated at NASA/ Langley Research Center using the etch-back epitaxy process. The n-type GaAs substrates were Si doped to a carrier concentration of 2×10^{17} carriers/cm^3. The GaAlAs layer thickness was between 0.3 and 0.5 μm. The pGaAs layer was approximately 1-μm thick, giving a junction depth of 1 μm (as measured from the GaAlAs interface). Large area, vacuum-evaporated, Sn-Ag contacts were used for electrical connections to the nGaAs. Front finger contacts were deposited to the GaAlAs layer by

sputtering a layer of Pd followed by a layer of Ag using an appropriate mask.

Before operating the solar cells at a high temperature, two GaAlAs-GaAs solar cells were prepared in order to test the stability of the solar cells upon heating. The purpose of the stability check was to obtain the open circuit voltage change due to the current leakage during the heat treatment procedure. There was no observable change in the open circuit voltage, short circuit current, or fill factor.

The solar cells were mounted on stainless steel headers and were given an antireflection coating. Before they were heat treated, their photovoltaic properties were measured and recorded. Heat treatment studies at 200° C were conducted by separating the solar cells from the headers and placing them in a vacuum oven for approximately 5 hours. During the heat treatment of these solar cells, the temperature was continuously recorded. After heat treatment the samples were remounted on the stainless steel headers and the photovoltaic properties were recorded. In particular, the open circuit voltage, short circuit current, fill factor, efficiency, spectral responses, and dark current voltage were measured both before and after heat treatment. The cells tested proved to be stable.

For the study of high-temperature operation of GaAs solar cells, a small electric heater together with a stainless steel header mounting plate and chromel-alumel thermocouple wires were prepared and installed in a small, blackened, stainless steel cylindrical chamber. Desired temperatures were obtained by adjusting the current input with two variacs. Alumina and titanium oxide were used to blacken the stainless steel cylindrical chamber in order to reduce reflection of light. The proper electrical insulation was achieved by using Al_2O_3. During the measurements, the solar cells were placed in a stainless cylindrical chamber with a quartz glass window which allowed the solar cells to be irradiated. A thermocouple wire was attached underneath to the stainless steel header plate in order to monitor the temperature during each measurement. Dry argon was slowly flushed into the system in order to maintain a small positive pressure to prevent the solar cell junction from oxidation. The temperature measurements on the solar cell were carefully calibrated

with special equipment designed in the laboratory. The temperature stability was maintained with less than ±1° C during the measurements.

Since silver epoxy was not adequate for the solar cell operation at the temperatures above 180° C, the thermal compression bonding technique was employed for sample mounting and electrical contacts. Usually 3 to 4 gold wires having a 2-mil diameter were used to attach the cell to the header. Before mounting the cell on the header, the headers were coated with a thin gold film for better adhesion. The heat conduction through the gold wire to the solar cell was carefully observed by monitoring the temperature on the header and on the solar cell junction. During all measurements, sufficient time was allowed for the solar cell to establish itself at an equilibrium temperature.

Measurements were repeated and the reproducibility of the measurements was maintained. For the illuminated current-density voltage measurements, a solar simulator light source was used to produce an input power of 135.3 mW/cm^2 at AMO. For the dark current density voltage measurements, the V_{oc}-J_{sc} method was employed in order to reduce the effect of the series resistance.

The spectral responses as a function of temperature were measured using a mercury lamp, electrometer, and a set of narrow band pass filters. The mercury lamp was chosen in order to obtain a strong light intensity for all wavelengths. This also helped to compensate for the increasing dark current with increasing temperature and thereby produce enough current density at high temperatures for measurement. To achieve monochromatic light, a series of narrow band pass filters with approximately 50 Å resolution was used. The current and photon density were recorded at each wavelength, enabling us to obtain absolute spectral responses. Measurements were repeated several times for each solar cell in order to ensure maximum accuracy. The wavelengths chosen for the spectral responses were from 0.44 μm to 1 μm with 0.04 to 0.05-μm wavelength intervals and temperatures ranging from 28° C to 346° C with approximately 60° C incremental steps. The absolute spectral responses were numerically integrated to produce the current density J_{sc}, which was then compared with the J_{sc} obtained from the illuminated J-V measurements. The obtained values for the current densities were well within

the error range involved in the approximation. All the measurements were repeated, and reproducibility was carefully checked at each time of the run.

Light Current Voltage Curves

The current voltage (J-V) characteristics under AM0 sunlight for GaAlAs-GaAs solar cells in the temperature range from 27° to 350° C were studied. Similar measurements were made by Hovel (ref. 11) by employing a xenon light source in the temperature range from 27° to 245° C. In the past, the values of illuminated photovoltaic characteristics above T = 245° C were obtained by extrapolation. This was because of the experimental difficulties encountered at temperatures above T = 245° C (refs. 11, 12). In this study we extended the temperatures beyond T = 245° C and made actual measurements of illuminated photovoltaic characteristics of GaAs solar cells up to a temperature of T = 350° C. For these measurements the solar simulator was used to reduce the excessive intensity of light at 0.82 μm. The measurements obtained were not corrected for the contact area masking.

Figure 1 summarizes the light current voltage curves for temperatures in the range from 27° to 350° C. The rest of the cells tested exhibited a similar behavior. The following are some nominal values recorded at 27° C: V_{oc} = 0.97 V, FF = 0.7, J_{sc} = 24 mA/cm^2, and efficiency = η = 12 to 14 percent. Using TiO_2 antireflection coating, the J_{sc} increased to 33 mA/cm^2 and the efficiency η rose to nearly 16 percent. As the temperature of the solar cell increased, the open circuit voltage decreased due to the dark current increase. The rate of change for V_{oc} over the entire temperature range was observed to be $\Delta V/\Delta T$ = -2.2 mV/°C for all solar cells tested. This value is in agreement with previous measurements (ref. 11). We also observed that the short circuit current density increased with increasing temperature, but not in the manner reported earlier (ref. 11). The short circuit current density changed with increasing temperature in the following manner: the short circuit current density increased with increasing temperature due to the improvement in the diffusion length and a shift in the absorption edge to lower energies. The short circuit currents at 27° C for all solar cells were

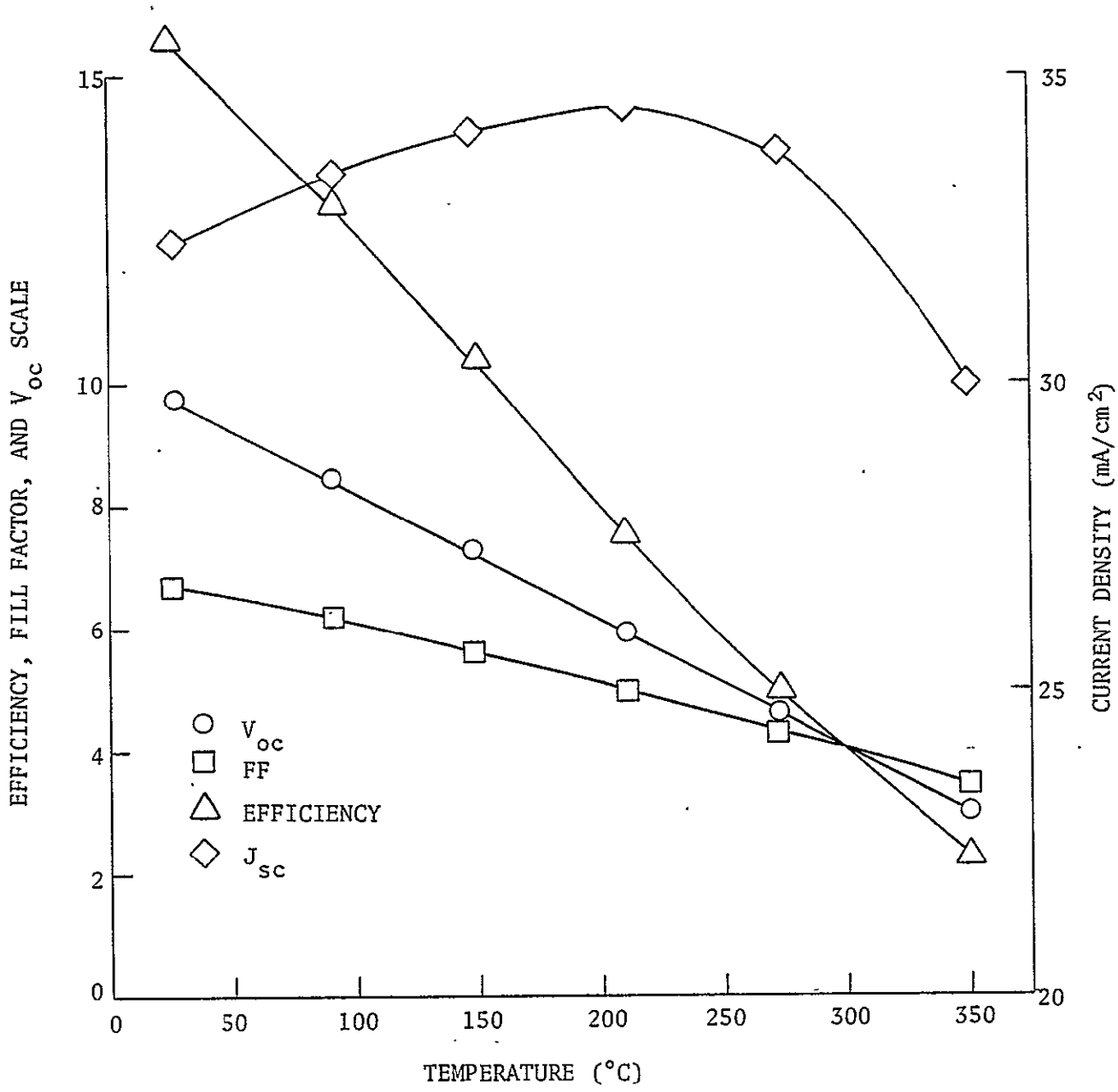

Figure 1. Photovoltaic parameters as a function of temperature.

observed in the neighborhood of 24 mA/cm^2. The short circuit current gradually increased with increasing temperature up to around 210° C. Then, for temperatures above 210° C, the short circuit current density slowly decreased with increasing temperature. At temperatures above 270° C, there was a considerable decrease in the short circuit density. Figure 2 demonstrates that the spectral response at 346° C was reduced. This reduction could be attributed to an increased dark current or to contact resistance. In general our measurements for the change in short circuit current density with temperature $\Delta J_{sc}/\Delta T$ showed much smaller rates than that obtained in reference 11. In the temperature range 27° C to 210° C we observed that $\Delta J_{sc}/\Delta T = 2\ mA/cm^2$.

For most solar cells the fill factor at 27° C was in the neighborhood of 0.65 to 0.7, as compared to 0.78 in reference 11. As temperature increased, the fill factor decreased, and at T = 350° C we found the fill factor to be around 0.35.

The efficiency at 27° C was between 12 and 14 percent for most of the solar cells tested. We observed that the efficiency changed with temperature and decreased at the rate of 0.035 percent/°C. This value is slightly higher than the rates of 0.02 to 0.03 percent/°C reported in reference 11. For our measurements, the small improvement in the short circuit current density did not offset the linear decrease of the open circuit voltage with increasing temperature. Accordingly, the efficiency decreased linearly with increasing temperature. The measured efficiency at 350° C for most solar cells with antireflection coatings was in the neighborhood of 2 percent. The GaAlAs-GaAs solar cells were usable at and up to the temperature of T = 350° C, but the measured values of efficiency were lower than the predicted values obtained from the extrapolation of earlier measurements (refs. 11, 12).

Dark Current Voltage Curves

The dark currents in GaAs solar cells are composed of injected majority currents over the potential barrier and the recombination current of holes and electrons within the depletion region. The dark current voltage characteristics are determined by the combined effects of the current transport mechanisms and series and shunt resistance.

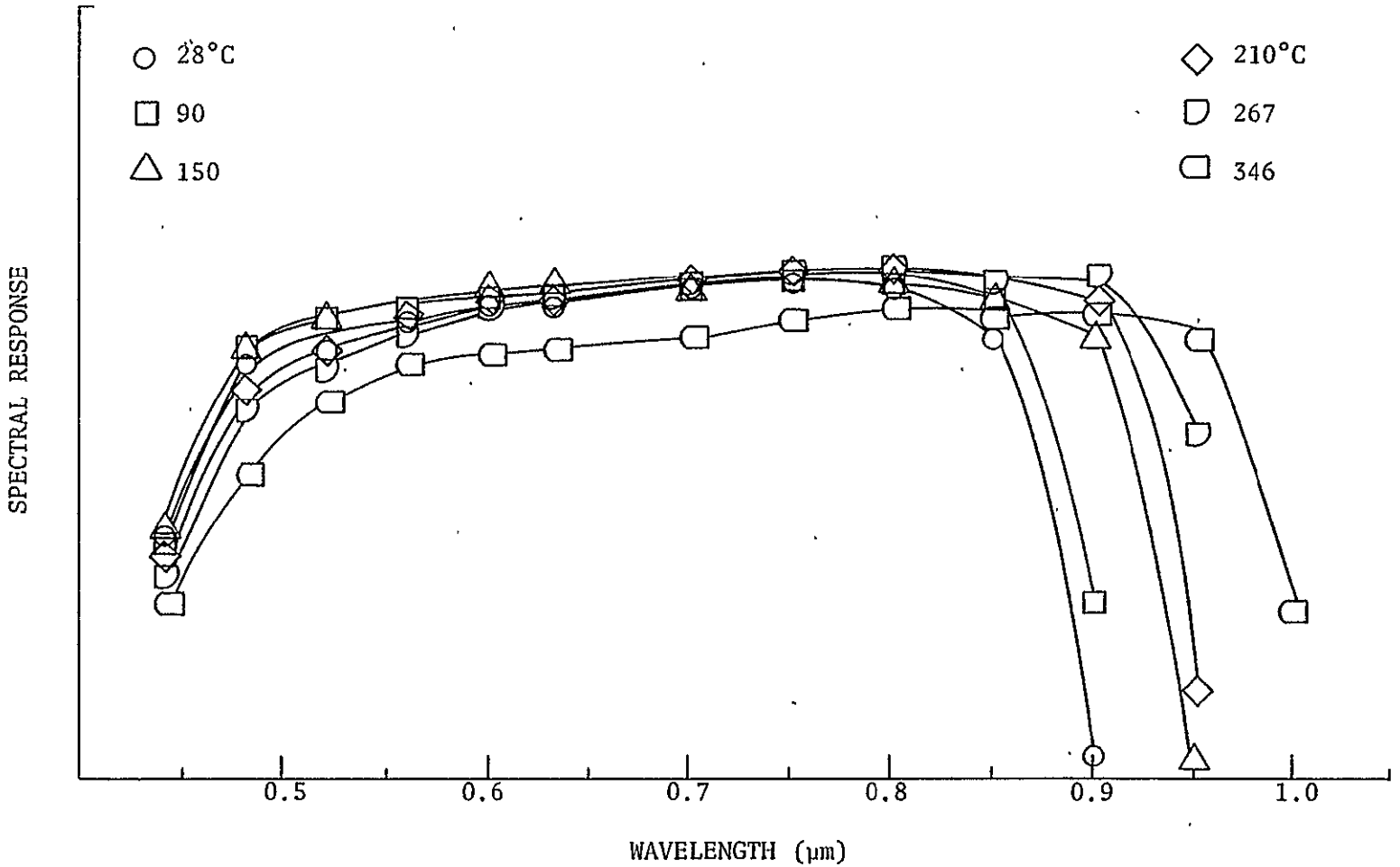

Figure 2. Measured spectral responses as a function of temperature.

The details of the dark J-V mechanisms are well described elsewhere (ref. 13). The injection currents vary as exp[qV/KT], and the recombination currents vary as exp[qV/2KT]. Accordingly, the recombination currents dominate at a low forward bias, and the injection current dominates at a higher bias. For a high band gap material such as GaAs, the recombination current is generally greater than the injection current. As the temperature increases, the intrinsic carrier density increases due to the band gap decrease. The dark current largely determines the voltage output. Hence, with increasing temperatures, the output voltage decreases due to the increasing intrinsic carrier densities.

The data collected was obtained using the V_{oc}-I_{sc} method. This method minimizes the effect of the series resistance on the measured currents and voltages. The current voltage data as a function of temperature is illustrated in figure 3. Most measurements show two exponential regions exist which indicate the two different current components. The slope of the J-V curves determines the diode A-factor and saturation current density J_o at zero bias. An A-factor of A = 2.1 was obtained for most solar cells at room temperature. In general, the A-factor obtained from the experimental data was slightly higher than the predicted value. Some solar cells had an A-factor as high as A = 2.6. This high an A-factor indicates the existence of poor diode characteristics. Metal precipitation, oxygen, and native defects are partially responsible for this high an A-factor value. During this study, the A-factor and J_o values were determined by single exponential least squares curve fitting of the data, for which the mean square difference between the measured and computed values was minimized. The A-factor values and J_o values thus obtained are given in figure 3. The A-factor values decrease from 2 to 1.6 with increasing temperature. This is to be expected since the ideal diode A-factor is expressed as

$$A \simeq \frac{q}{KT} \frac{1}{\frac{\Delta \ln J}{\Delta V}} \tag{1}$$

where Δ is the difference between two data points.

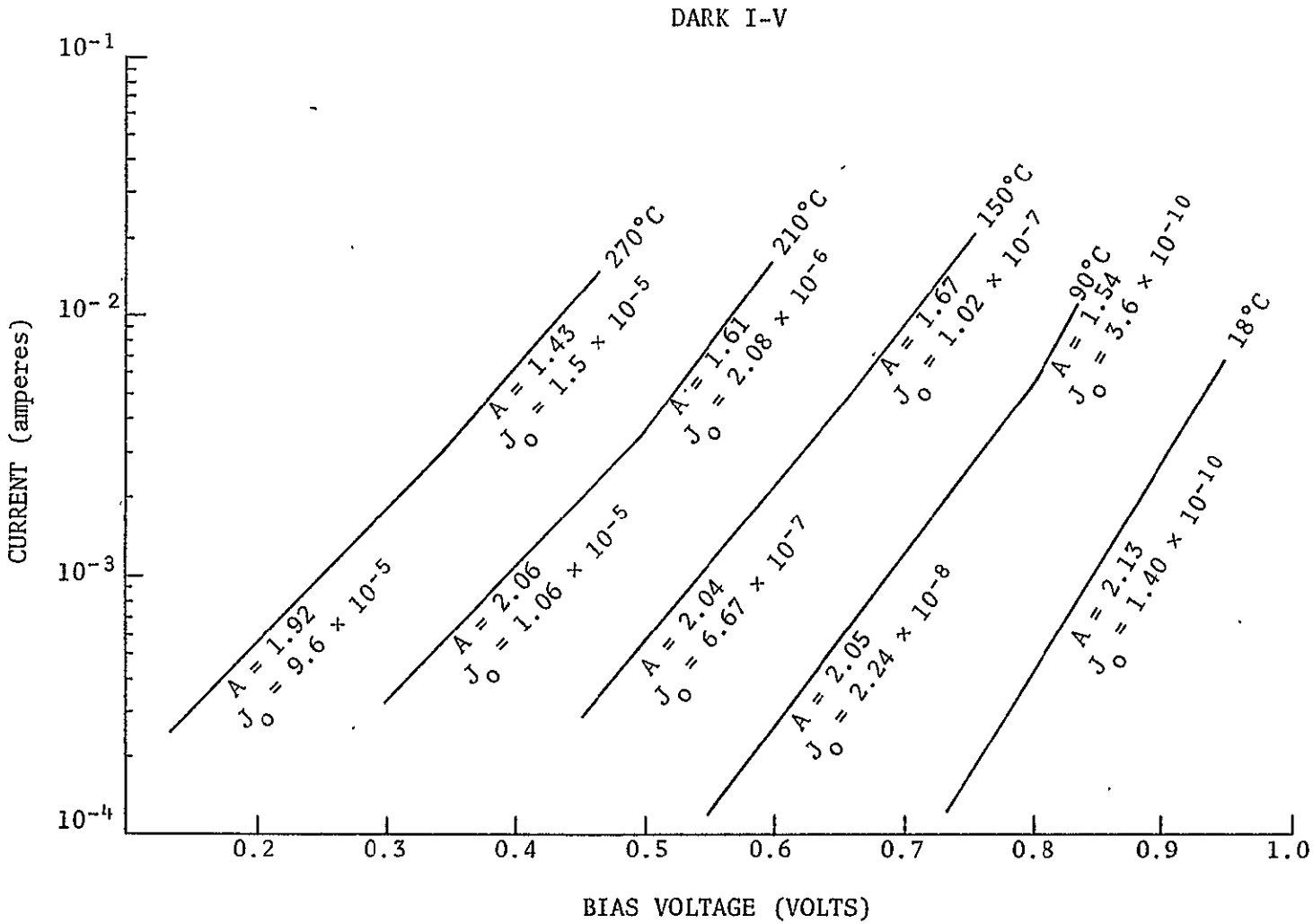

Figure 3. Dark J-V as a function of temperature.

Since the data indicates that the recombination current is dominant, a composite lifetime τ_c as a function of temperature can be obtained (ref. 14) as

$$\tau_c = \frac{qn_i W}{2J_o} \tag{2}$$

where J_o is the saturation current density, n_i is the intrinsic carrier density, and W is the width of the depletion region. The depletion region can be obtained from the known doping density. The temperature-dependent value of W was calculated assuming a slowly varying dielectric constant. The depletion region is approximately 0.1 μm at T = 27° C. With increasing temperature the depletion region decreases to 0.08 μm. Using equation (2), the composite lifetime at 18° C is approximately $2(10^{-9})$sec. Summarized in table 2 are the composite lifetimes (as a function of temperature) deduced from the dark J-V curves.

Table 2. Recombination lifetime deduced from dark J-V as a function of temperature.

Temperature (°C)	Lifetime (sec)
18	2.31×10^{-9}
90	1.75×10^{-8}
150	5.9×10^{-8}
210	7.4×10^{-8}
270	1.04×10^{-7}
350	1.55×10^{-7}

This composite lifetime (ref. 14) is a weighted average of the minority carrier lifetimes in the p and n materials. In the next section these composite lifetimes will be compared with lifetimes obtained by fitting the spectral response data.

Spectral Response Curves

The spectral responses of the GaAs solar cells were measured at different wavelengths and different temperatures. The experimental data obtained was read by an HP9830 calculator to produce the measured absolute spectral responses. The measured spectral responses were observed to be flat between the 0.55 μm and 0.85 μm wavelengths for all temperatures considered.

In order to ensure that we had absolute spectral response measurements, we numerically integrated the spectral response curve with the solar spectrum over the entire wavelength in order to obtain the current density J_{sc}. The value of J_{sc} obtained in this way agreed within 10 percent with the current density obtained from the illuminated current voltage data. The small discrepancy between the measurements was probably caused by the approximate integration procedure used over the entire wavelength.

The change in the spectral response at the blue end of the spectrum, with increasing temperature, was small when compared to the spectral response change at the red end of the spectrum. The spectral response in the intermediate wavelength regions lying between the blue and red regions was essentially a constant. The current, in the red end of the spectrum, increased with increasing temperature due to the band gap reduction with increasing temperature. However, the spectral response with increasing temperature did not significantly affect the total current. These measurements give the complete spectral response as a function of temperature for the first time.

In order to explain the measured spectral response curves with increasing temperature, we used the Hovel model for the spectral response as developed in reference 15. In this analytical model for the spectral response we made many assumptions. Since the absorption coefficient of AlGaAs as a function of temperature is not known, we assumed that this absorption coefficient (along with the absorption coefficient of GaAs) behaved like the band gap of GaAs as a function of temperature. The following temperature relationships were also employed in the model.

$$D \propto T^{-1/2}, \quad \mu_p \propto T^{-3/2}$$
$$\tau \propto T^{3/2}, \quad \mu_n \propto T^{-3/2} \qquad (3)$$
$$L \propto T^{1/2}$$

where D is the diffusion coefficient, τ is the lifetime, L is the diffusion length, T is the temperature in degrees Kelvin, and μ_p, μ_n are mobilities.

The calculated spectral responses were compared with the measured spectral responses. The best fits of the experimental spectral responses as a function of temperature are illustrated in figures 3 and 4. The parameters used in the best fit model are summarized in table 3. The parameters that are critical in fitting the blue end of the spectrum are the aluminum composition, the recombination velocity, the diffusion length, and lifetime in the AlGaAs. At the red end of the spectrum, the parameters most important are the hole diffusion length and lifetime. In general, there was good agreement between measured and calculated spectral responses. The band gap of AlGaAs as a function of temperature as well as aluminum content in AlGaAs and surface recombination velocities in AlGaAs and pGaAs must be accurately determined to further reduce the error in fitting the spectral response curves at the blue and red ends of the spectrum.

Various solar cell parameters were estimated in obtaining the computer fits to the experimental data. These values are given in table 3. Note that the recombination lifetime was also obtained in this way from the spectral response measurements. The value obtained for the lifetime by this method differed by a factor of 10 from the composite lifetimes calculated earlier.

THEORETICAL MODELS FOR HIGH-TEMPERATURE OPERATION OF $Ga_{1-x}Al_xAs$-GaAs SOLAR CELLS

In this section we present some theoretical models for the high-temperature operation of GaAs solar cells. This section is based upon the discussions found in reference 16 through 20.

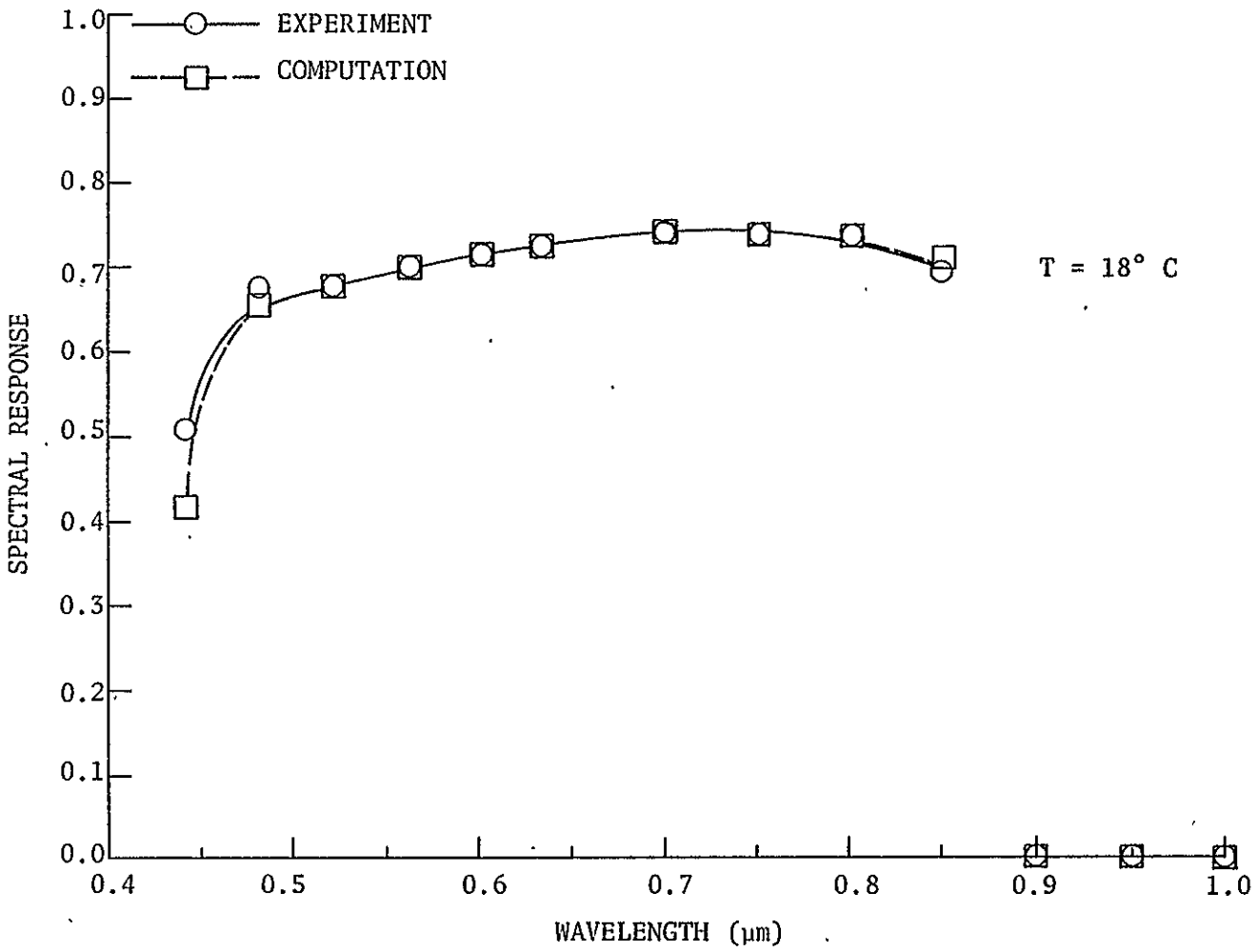

Figure 4. Spectral response curves at various temperatures.

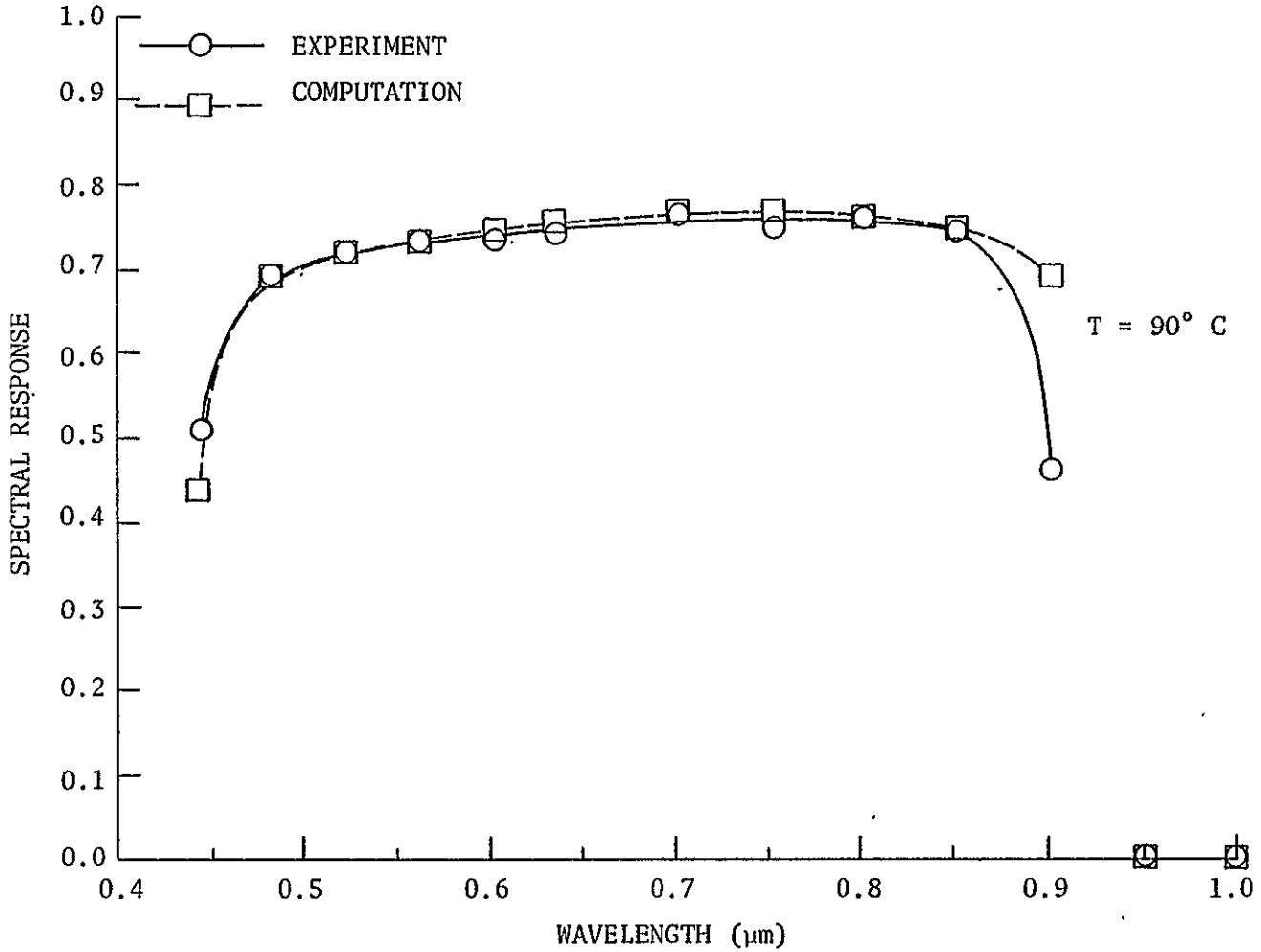

Figure 4. Continued.

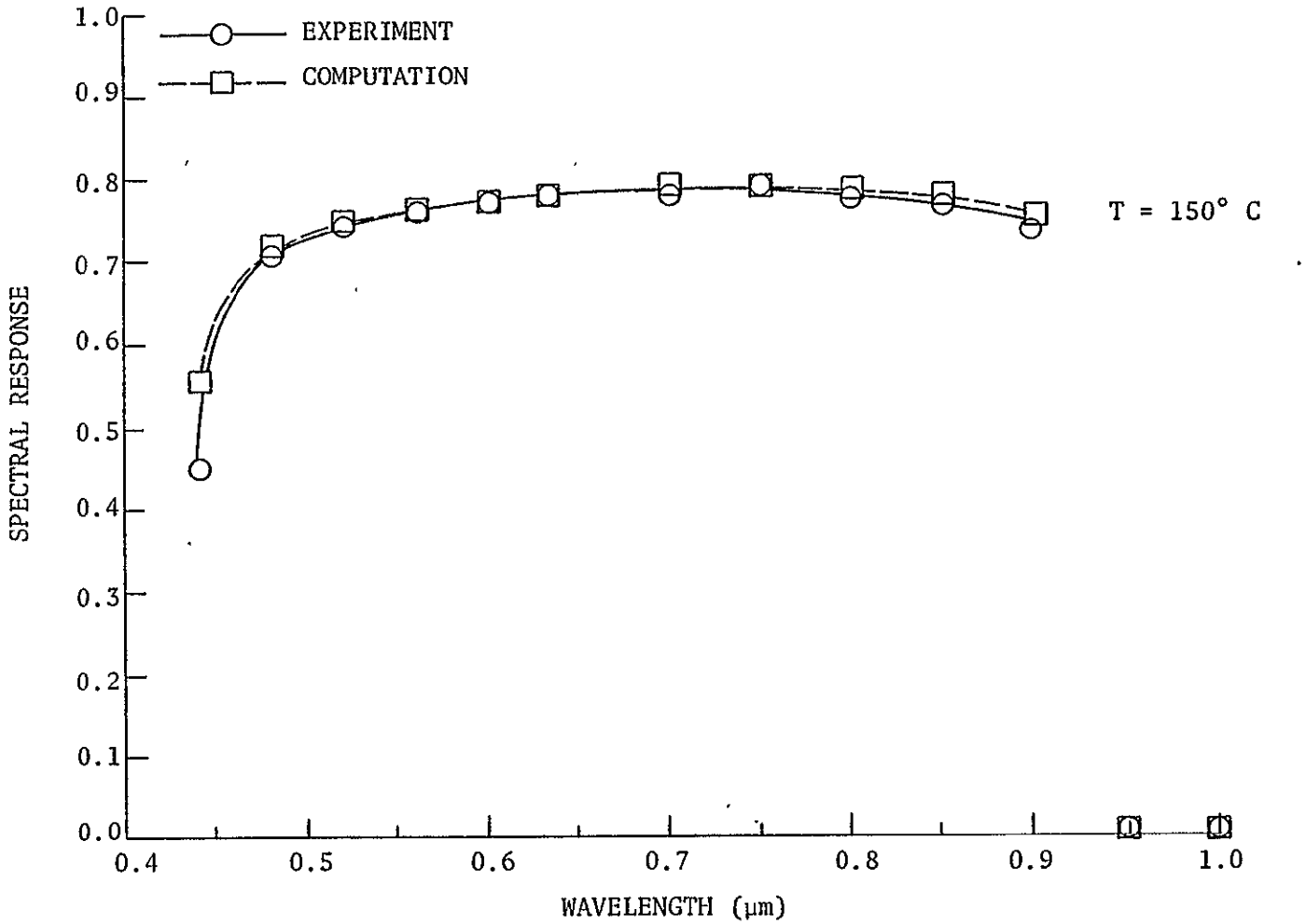

Figure 4. Continued.

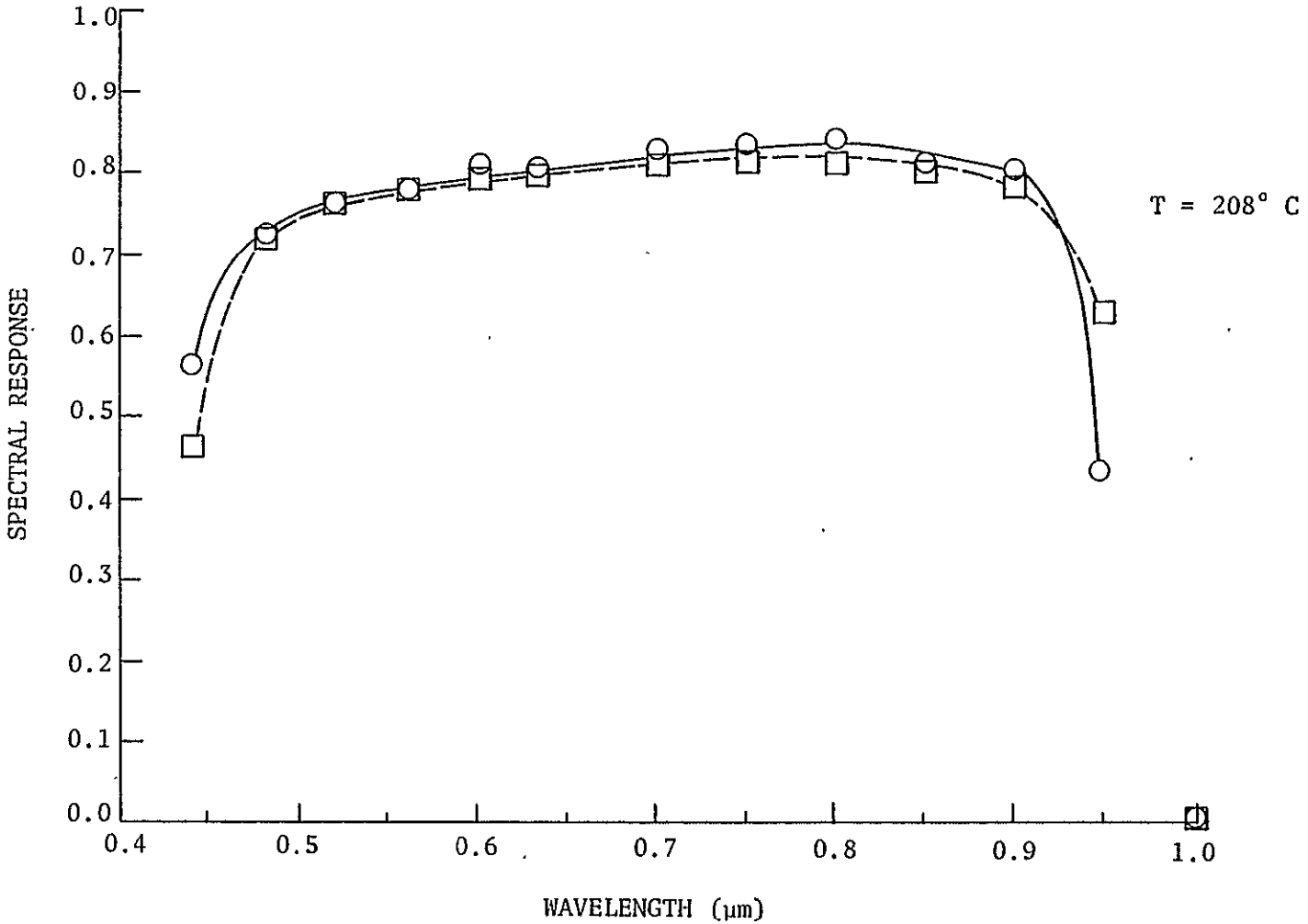

Figure 4. Continued.

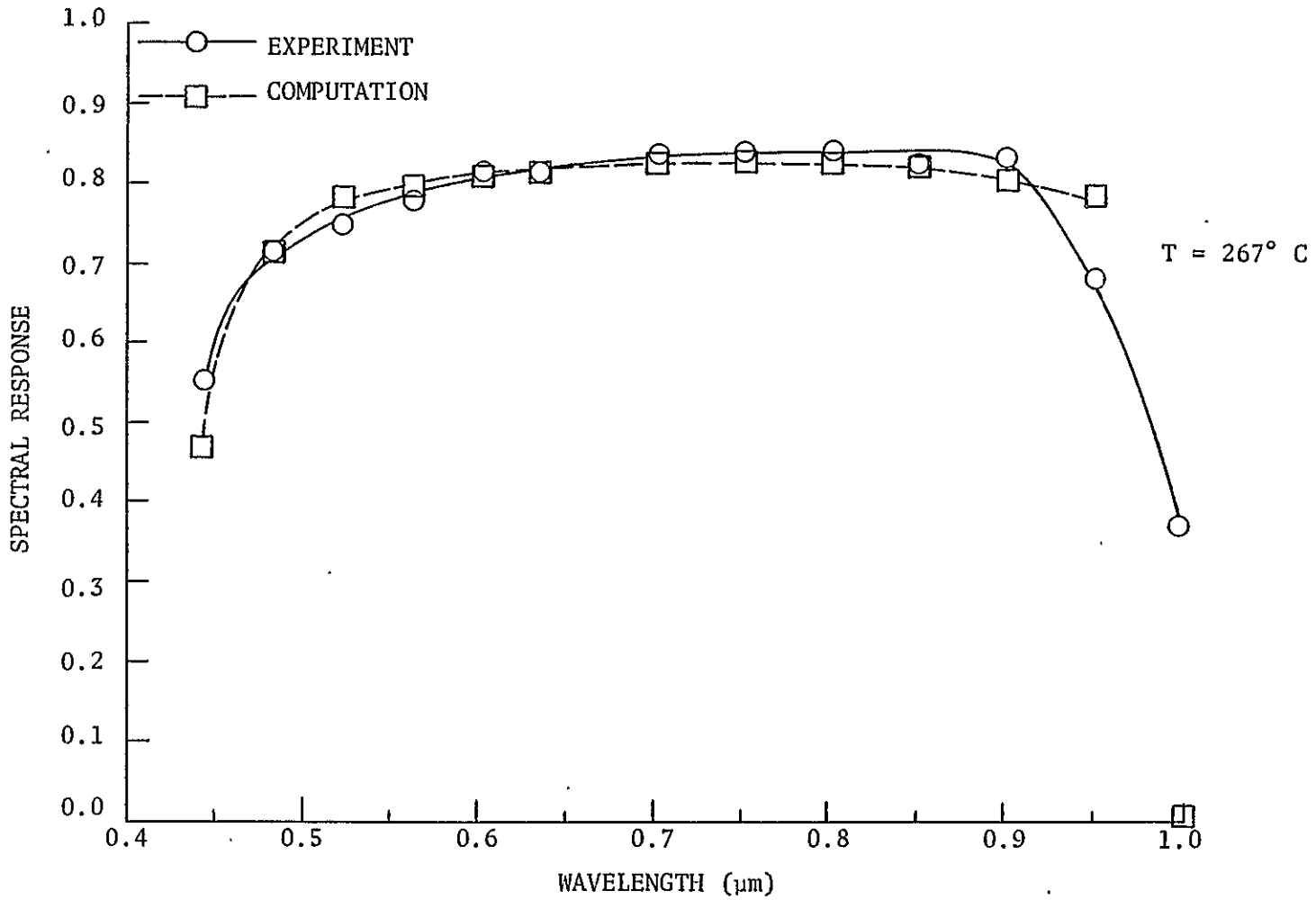

Figure 4. Continued.

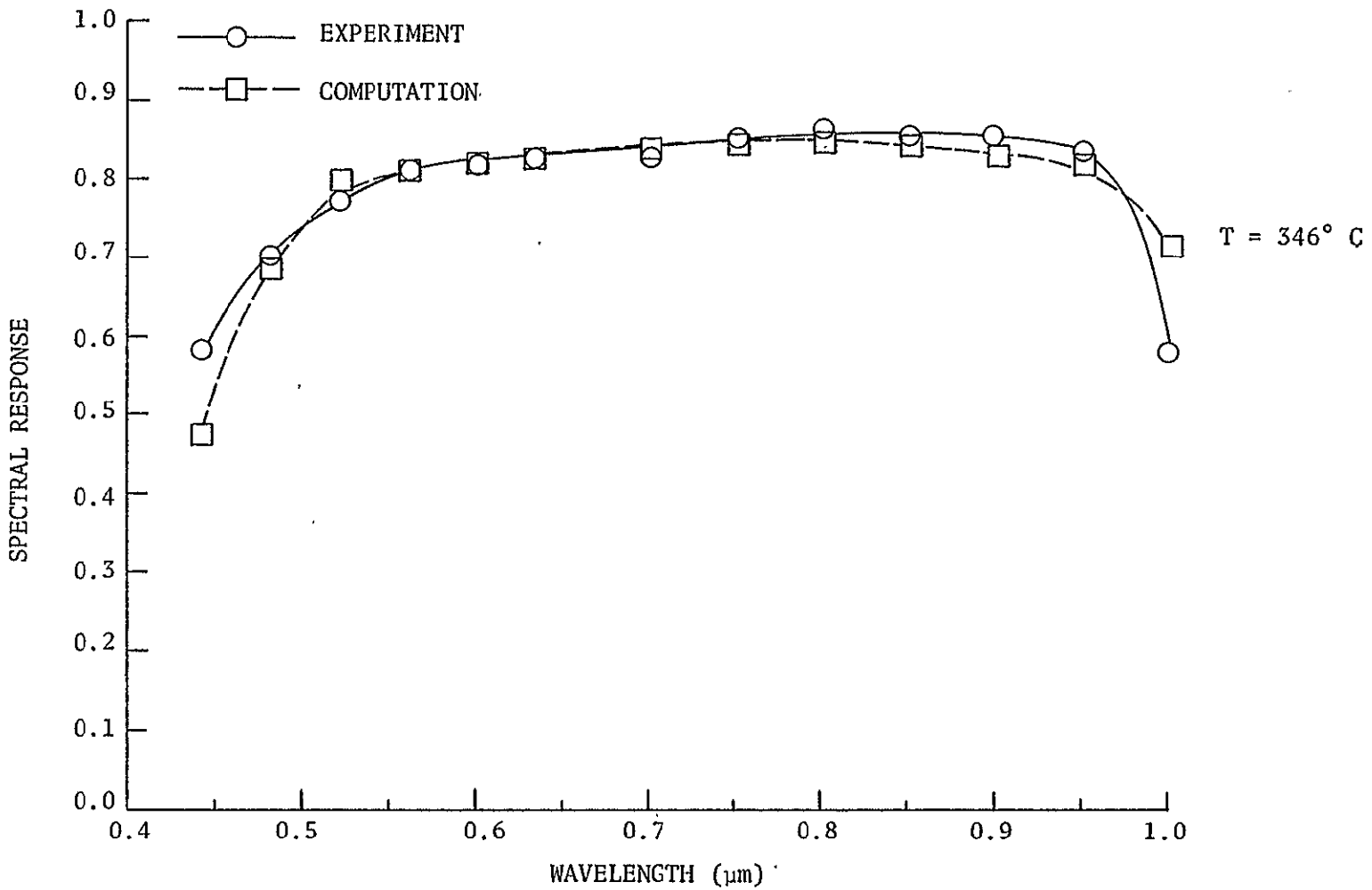

Figure 4. Concluded.

Table 3. Parameters deduced from temperature-modeled spectral responses.

Temperature (°K)	τ_a (sec) L_a (cm)	D (cm^2/volt-sec)	τ_g (sec) L_g (cm)	D (cm^2/volt-sec)	τ_p (sec) L_p (cm)	D (cm^2/volt-sec)
300	1×10^{-7} 2.5×10^{-5}	6.25×10^{-3}	1.13×10^{-10} 1.0×10^{-4}	88.70	4.66×10^{-9} 1.90×10^{-4}	7.75
363	1×10^{-7} 2.5×10^{-5}	6.25×10^{-3}	1.50×10^{-10} 1.1×10^{-4}	80.62	6.20×10^{-9} 2.09×10^{-4}	7.04
423	1×10^{-7} 2.5×10^{-5}	6.25×10^{-3}	1.89×10^{-10} 1.19×10^{-4}	74.68	7.8×10^{-9} 2.26×10^{-4}	6.52
481	1×10^{-7} 2.5×10^{-5}	6.25×10^{-3}	2.29×10^{-10} 1.27×10^{-4}	70.04	9.95×10^{-9} 2.40×10^{-4}	6.12
540	1×10^{-7} 2.5×10^{-5}	6.25×10^{-3}	2.72×10^{-10} 1.34×10^{-4}	66.099	1.13×10^{-8} 2.55×10^{-4}	5.78
619	1×10^{-7} 2.5×10^{-5}	6.25×10^{-3}	3.34×10^{-10} 1.44×10^{-4}	61.74	1.38×10^{-8} 2.73×10^{-4}	5.39

Fixed Parameters Used for Calculation

$S_a = 10^6$ cm/sec

$S_g = 10^4$ cm/sec

Hole density = 2×10^8

Electron density = 1.3×10^{17}

Window thickness = 0.3 μm

Junction depth = 1 μm

x in $(Al_xGa_{1-x})As$ = 0.95

The interaction of electron irradiation with the GaAs solar cell produced displacements of atoms within the crystal lattice. The fraction of these displacements which remain after long periods of time at room temperature is called "permanent damage." The process of annealing point defects involves their diffusion in the lattice until they encounter traps or sinks where they will then cease their meandering within the crystal.

In the electron irradiation of semiconductor crystals, coulomb scattering events will occur and the electrons will transfer some of their energy to the lattice atoms. The maximum amount of energy that can be transferred is given by (ref. 16)

$$T_m = \frac{2(E_e + 2m_e c^2)E_e}{Mc^2}$$

where E_e = electron energy, m_e = electron mass, c = velocity of light, M = lattice atom mass. For a GaAs crystal the maximum energy that can be transferred by 1-MeV electrons is

$$T_m,Ga = \frac{2[1 + 2(0.510577)](1)}{64890.442} = 62.294 \text{ (eV)}$$

$$T_m,As = 2\left[\frac{1 + 2(0.510577)}{69731.724}\right](1) = 57.969 \text{ (eV)}$$

Due to long-range interaction of coulomb collisions, the average amount of energy transferred to the lattice is less than these theoretical maximum values. There is a certain displacement threshold energy E_d which will displace a lattice atom to an interstitial position. This energy is between 10 and 60 eV for most semiconductor materials. The displaced atoms will leave behind a vacancy in the crystal lattice, and the resulting interstitial vacancy pair is called a "Frenkel defect." For most semiconductors these defects are produced uniformly throughout the crystal lattice. The total number of defects produced by an electron irradiation is a function of the electron energy and can be expressed as

$$N = \sigma_d N_\ell \phi \tag{6}$$

where

N = the total number of defects/cm^3

σ_d = the effective displacement cross section (cm^2), which is a function of electron energy (see fig. 5)

N_ℓ = the number of lattice atoms/cm^3

ϕ = the electron fluence (e/cm^2)

As defects are produced, various electrical characteristics and responses of the GaAs solar cell are degraded. Annealing is the process of raising the temperature of the solar cell in order to impart an activation energy to the defects so that they become mobile within the crystal and will meander through the lattice seeking to obtain a lower energy state. Defects are removed by this annealing, and electrical properties that were degraded by the creation of defects are restored by the removal of defects. The amount of restoration in the electrical properties depends upon the annealing time and the annealing temperature.

The annealing of GaAs is essentially in two stages: (1) The Ga atoms require a fairly low activation energy which is around room temperature (27° to 127° C), and at this annealing temperature the interstitial-vacancy pairs combine and destroy each other. (2) The remaining damage is to the arsenic atoms which are displaced. These atoms require annealing around 240° C (513° K) in order to receive the activation energy necessary to become mobile. The annealing process at temperatures greater than 240° C is fairly complex as can be illustrated by considering the various reactions that can occur during the different stages of annealing.

We let

V_1 = vacancy

V_2 = di-vacancy

V_n = cluster of n-vacancies

i_1 = interstitial

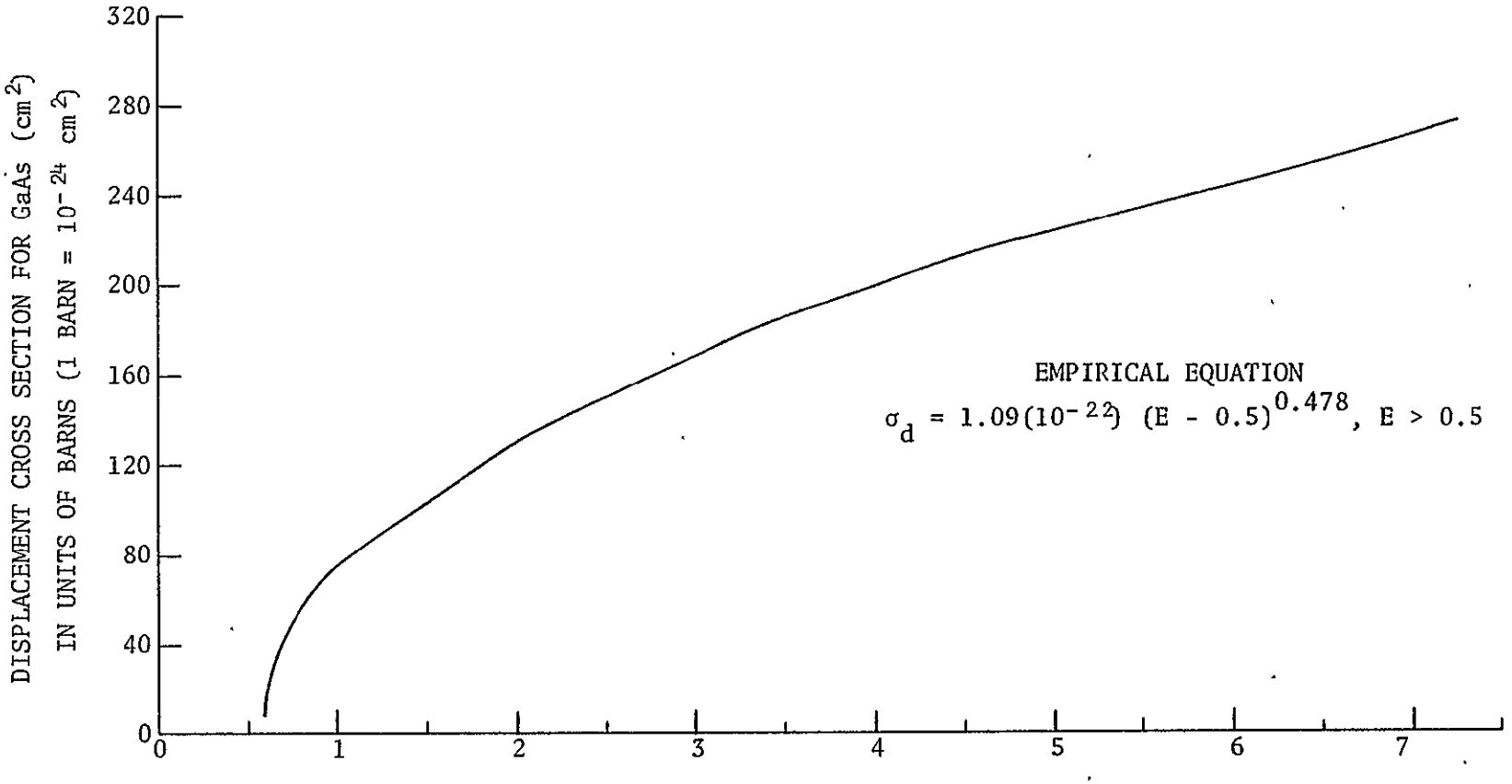

Figure 5. Displacement cross section σ_d as a function of electron energy.

i_n = cluster of n-interstitials

K_j = reaction constants (rates),

then the annealing kinetics can be categorized by various types of reactions. Some of these reactions are

(a) Recombination reactions. -

(1) $V_1 + i_1 \xrightarrow{K_1}$ annihilation

(recombination of closely spaced vacancies and interstitials)

(2) $i_1 \xrightarrow{K_2}$ sinks

(3) $i_1 + i_1 \underset{K_3}{\overset{K_2}{\rightleftharpoons}} i_2$

(4) $i_1 + \text{impurity} \underset{K_5}{\overset{K_4}{\rightleftharpoons}}$ complex

(interstitials combining with impurities)

(5) higher order reactions.

(b) Reactions due to diffusion of defects within lattice.-

(1) $V_1 + V_1 \underset{K_1}{\overset{K_6}{\rightleftharpoons}} V_2$

(2) $V_1 \xrightarrow{K_8}$ sinks

(3) $V_2 \xrightarrow{K_8}$ sinks

(4) $V_1 + \text{impurity} \underset{K_{11}}{\overset{K_{10}}{\rightleftharpoons}}$ complex

(impurity atom can capture vacancies)

(5) higher order reactions.

(c) Clustering reactions.- In addition to the reactions stated in (a) and (b), the presence of impurities will suppress various annealing reactions. These higher order and more complex types of reactions are assumed to be secondary to the basic reaction of vacancies and interstitials annihilating each other.

With reference to figure 6, let N_D equal the number of defects produced by a 1-MeV electron fluence of ϕ (e/cm^2). Using equation (6) we have

$$N_D = \sigma_d N_\ell \Phi \tag{7}$$

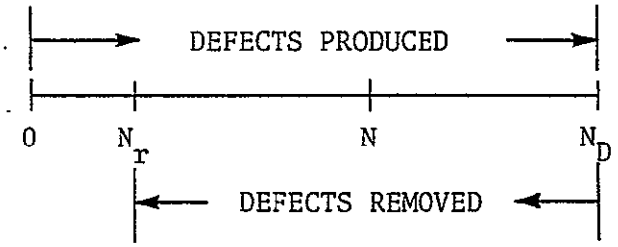

Figure 6. Defect production and removal.

Using t as time, $N = N(t)$ the defects at time t, T = temperature (°K), and N_r as the defects which remain after a long time, we assume that the recovery rate is proportional to the defects remaining. This assumption is analogous to assuming a first order or monomolecular chemical reaction between the vacancies and the interstitials. We write

$$\underbrace{\frac{d}{dt}(N_D - N)}_{\text{recovery rate}} = \underbrace{\omega_o e^{-\frac{E_a}{KT}}}_{\text{proportionality constant}} \underbrace{(N - N_r)}_{\text{defects remaining}} \tag{8}$$

where

N = number of defects at any time t of the annealing process

$N_D = \sigma_d N_\ell \phi$ = defects produced by fluence ϕ

$\omega_o e^{-E_a/KT}$ = Boltzmann factor with E_a = activation energy (eV), K is Boltzmann's constant, T is annealing temperature (°K), and ω_o is the frequency factor which represents the frequency at which vacancies and interstitials annihilate each other

N_r = defects remaining after a long anneal time.

The differential equation (8) is subject to the conditions $N(0) = N_D$ and $\lim_{t\to\infty} N(t) = N_r$. It is readily verified that the solution of equation (8) which satisfies the above conditions is

$$N = N(t) = N_r + (N_D - N_r) \exp\left\{-\omega_o t\, e^{-E_a/KT}\right\} \tag{9}$$

Let f denote the fraction of initial defects which is removed during an anneal time τ. For N_D = initial defects and $N = N(\tau)$ = defects remaining after an anneal time τ, we have

$$f = \frac{N_D - N(\tau)}{N_D} \tag{10}$$

or

$$N = N(\tau) = N_D(1 - f) \tag{11}$$

How defects are removed depends upon the type of reactions that take place. For a monomolecular reaction we have shown $N = N(\tau)$ is given by equation (9). For a bimolecular reaction, we can write

$$\frac{dN}{d\tau} = F - aN - bN^2 \tag{12}$$

where F, a, b are constants and τ is the annealing time.

Let

$$\omega = \sqrt{a^2 + 4bf} = \omega_o \exp\{-E_a/KT\}$$

then we may express equation (12) in the form

$$\frac{dN}{\left(N + \frac{a}{2b}\right)^2 - \frac{\omega^2}{4b^2}} = bd\tau \tag{13}$$

An integration produces the solution

$$N = N(\tau) = N_D \frac{\left\{(1 - A)e^{-\omega\tau} + \frac{N_r}{N_D}\left(1 - e^{-\omega\tau}\right)\right\}}{1 - Ae^{-\omega\tau}} \tag{14}$$

where $N(0) = N_D$ and $A = \left(N_D + \frac{a - \omega}{2b}\right)\Big/\left(N_D + \frac{a + \omega}{2b}\right)$ is a constant. This solution enables us to write equation (10) in the form

$$f = f_o\left(1 - e^{-\omega\tau}\right)\Big/\left(1 - Ae^{-\omega\tau}\right) \tag{15}$$

which represents the fraction of defects remaining in the case of bimolecular reactions. In the case where b tends to zero, then $\omega = a$ and $A = 0$ so that for monomolecular reactions equation (15) takes on the form

$$f = f_o\left(1 - e^{-\omega\tau}\right) \tag{16}$$

where $f_o = (N_D - N_r)/N_D$ is the fraction of defects remaining after a long time.

We now define ϕ_e as the equivalent fluence to produce N defects. Using equation (11) we may write

$$\phi_e = \frac{N(\tau)}{\sigma_d N_\ell} = \frac{1}{\sigma_d N_\ell} N_D(1 - f) \tag{17}$$

where $N = N(\tau)$ is a function of the annealing time τ and represents the number of defects remaining after an anneal time τ.

The following is a simplified annealing model. We start with the approximate relation (ref. 15)

$$\frac{I_{sc}}{I_{sco}} = \frac{F(\tau_{go}, S_{go}, L_{go}, X_j)}{F(\tau_g, S_g, L_g, X_j)} \tag{18}$$

where $F(\tau, S, L, X) = \frac{\tau_s}{L} \sinh\left(\frac{X}{L}\right) + \cosh\left(\frac{X}{L}\right)$ and

τ_{go}, τ_g are lifetimes (sec) before and after irradiation

S_{go}, S_g are recombination velocities (cm/sec) before and after irradiation

L_{go}, L_g are diffusion lengths before and after irradiation (cm)

X_j is junction depth (cm).

We assume further that the lifetime, recombination velocity, and diffusion length change with fluence according to the relations

$$\left.\begin{aligned} \frac{1}{\tau_g} &= \frac{1}{\tau_{go}} + D_g K_g \Phi_e \\ \frac{1}{L_g^2} &= \frac{1}{L_{go}^2} + K_g \Phi_e \\ S_g &= S_{go}\left(\frac{L_{go}}{L_g}\right)^2 \end{aligned}\right\} \tag{19}$$

where D_g is the diffusion coefficient and K_g is a damage coefficient (ref. 15). The quantity Φ_e, is the effective fluence defined by equation (17). Using equations (10), (15), and (17) we may write

$$\Phi_e = \Phi\left[1 - \frac{f_o\left(1 - e^{-\omega\tau}\right)}{\left(1 - Ae^{-\omega\tau}\right)}\right] \tag{20}$$

When equations (19) and (20) are substituted into equation (18), figures 7 through 13 result. The nominal values employed to produce these graphs are given in figure 9. In these curves we have used $\omega = \omega_o \exp(-E_a/KT)$ with $\omega_o = 2.8766(10^{12})$, $f_o = 0.94$.

As another way of predicting effects of annealing we will employ the following statistical models which were developed in reference 15 for 1-MeV electron fluences Φ and junction depths X_j (μm):

$$\log_{10}\left(\frac{I_{sco}}{I_{sc}} - 1\right) = 0.8649 + 0.194X_j + 1.075 \log_{10}\left(\frac{\phi}{10^{16}}\right) \tag{21}$$

and

$$\log_{10}\left(\frac{V_{oco}}{V_{oc}} - 1\right) = -0.6037 + 0.098X_j + \left[0.609 + 0.06 \log_{10}\left(\frac{\phi}{10^{16}}\right)\right] \times \log_{10}\left(\frac{\phi}{10^{16}}\right) \tag{22}$$

The current voltage relation for the solar cell is

$$I = I_{sc} - I_o\left[e^{\frac{qV}{A_o KT}} - 1\right] \tag{23}$$

where when $I = 0$, $V = V_{oc}$ = open circuit voltage and equation (23) gives

$$V_{oc} = \frac{A_o KT}{q} \ln\left[\frac{I_{sc}}{I_o} + 1\right] \tag{24}$$

where A_o is the A-factor (perfection factor), K is Boltzmann's constant, q is electron charge, I_{sc} is short circuit current, and I_o is the dark current. To incorporate annealing effects, we replace Φ in equations (21) and (22) with the equivalent fluence Φ_e defined by equation (20). In addition,

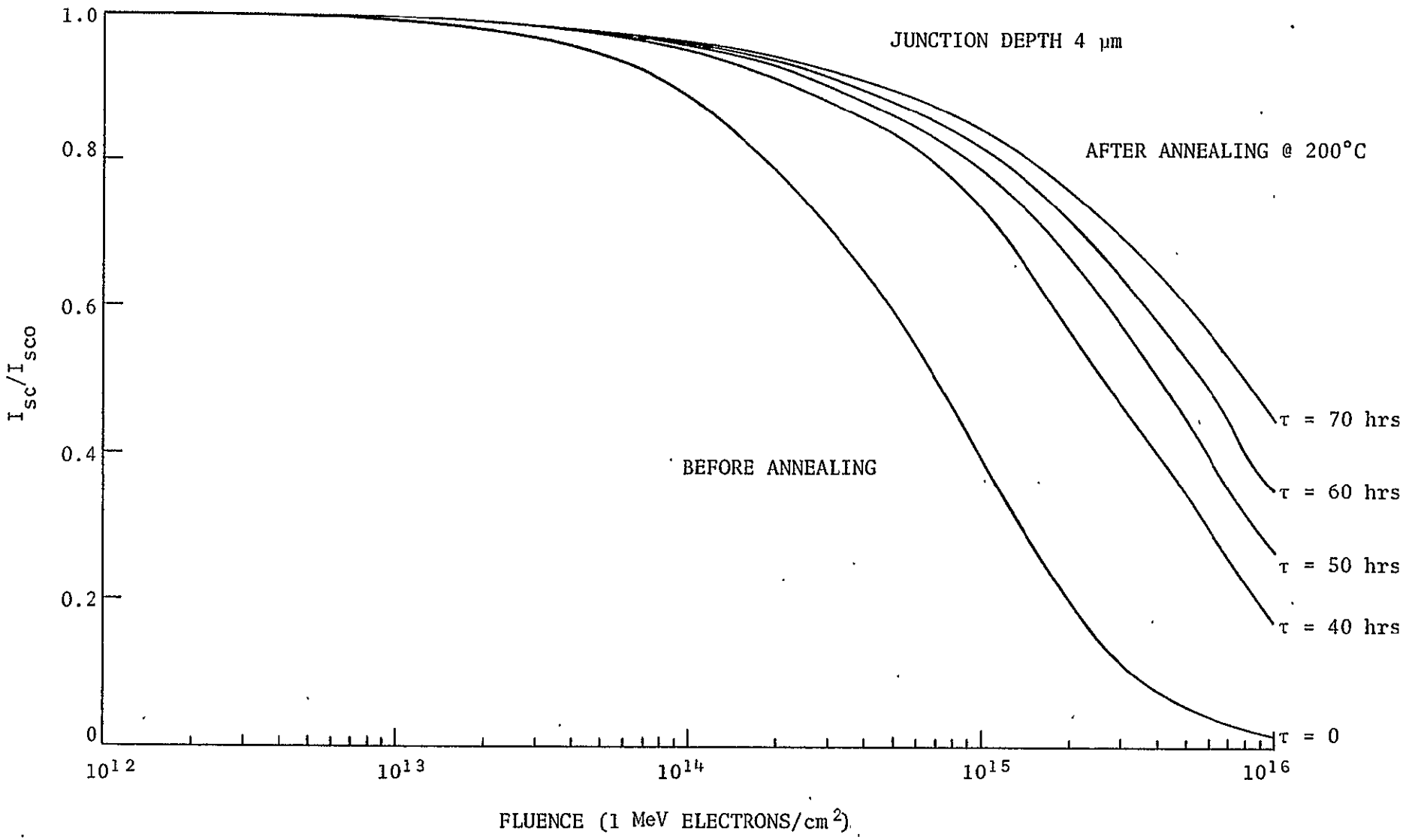

Figure 7. Short circuit current vs. fluence before and after annealing at 200°C for τ hours (theoretical curves A = 0).

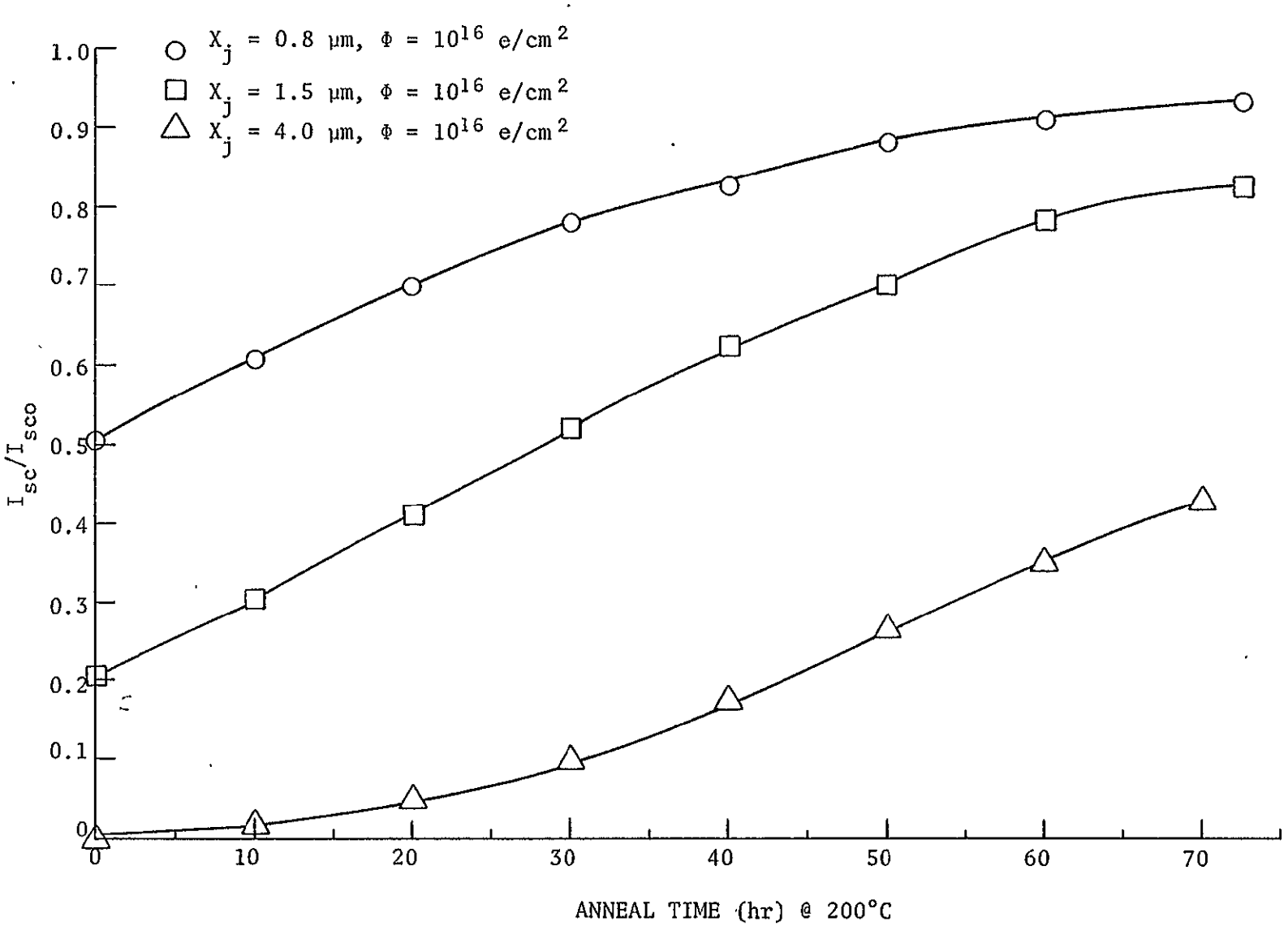

Figure 8. Short circuit current ratio vs. anneal time at 200°C (theoretical curves A = 0).

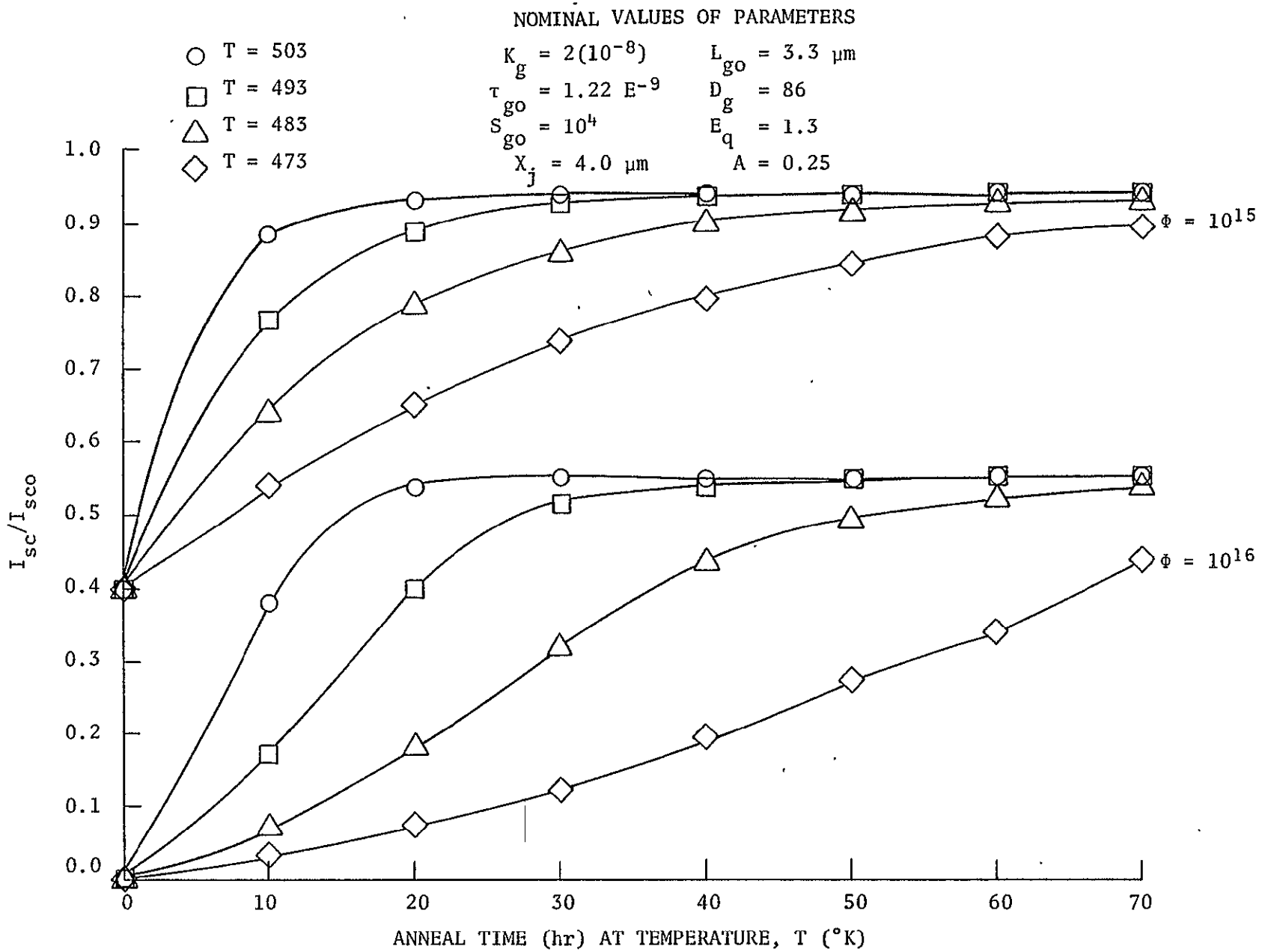

Figure 9. Short circuit current ratio vs. anneal time for various temperatures (theoretical curves).

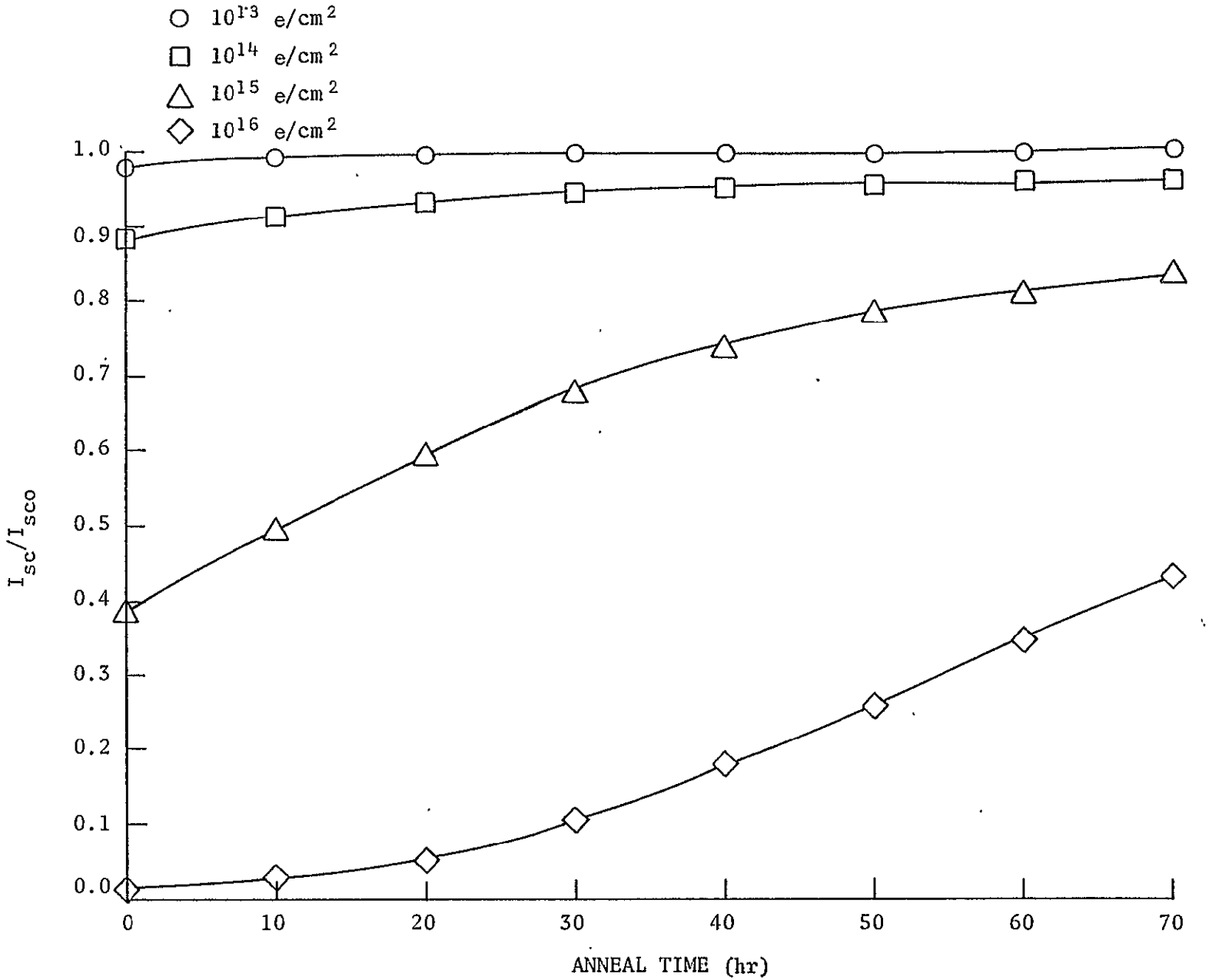

Figure 10. Annealing of deep junction (4-μm) cells at 200°C (theoretical curves A = 0)

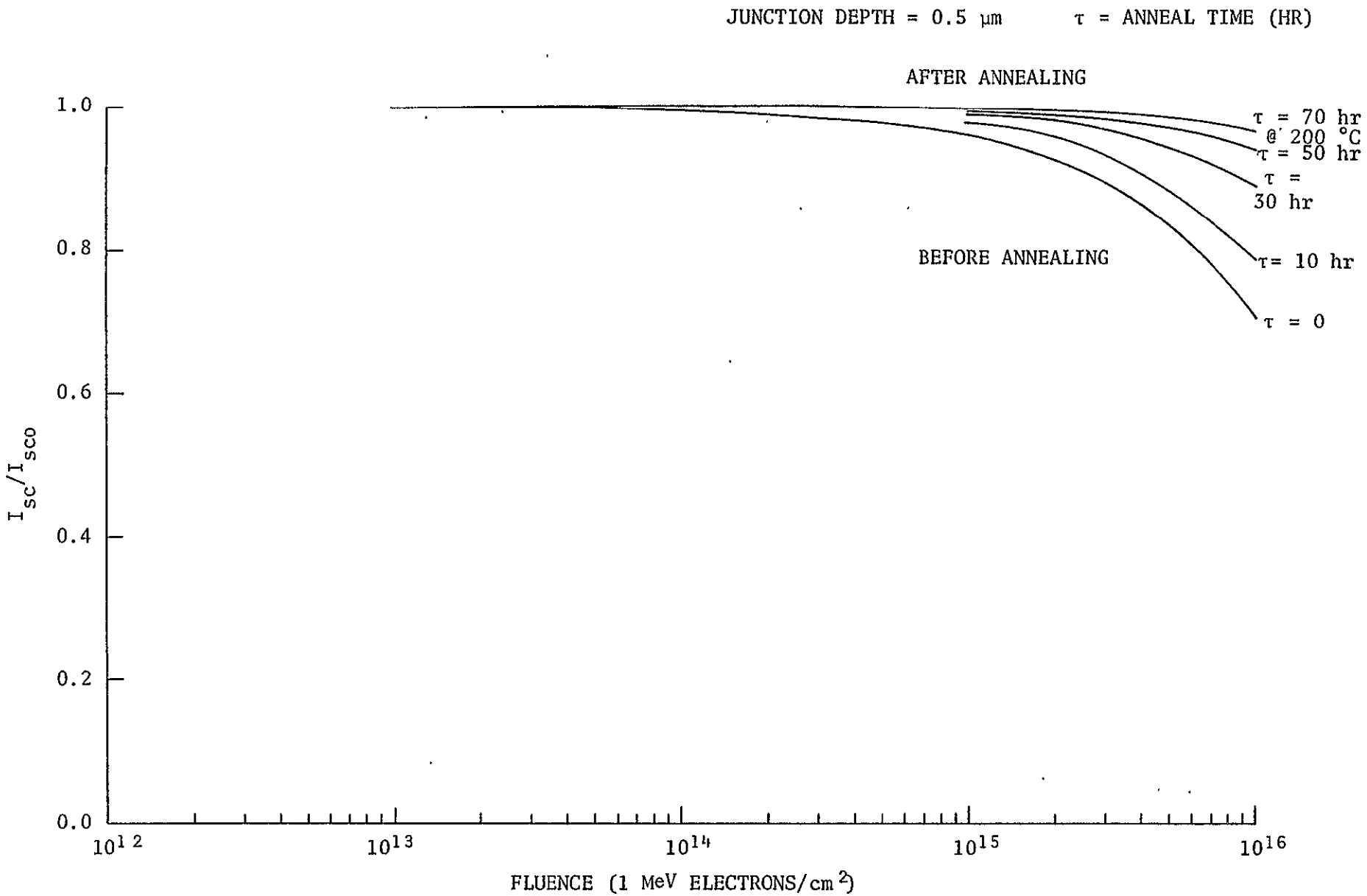

Figure 11. Annealing of shallow junction (0.5-μm) cells at 200°C (theoretical curves A = 0).

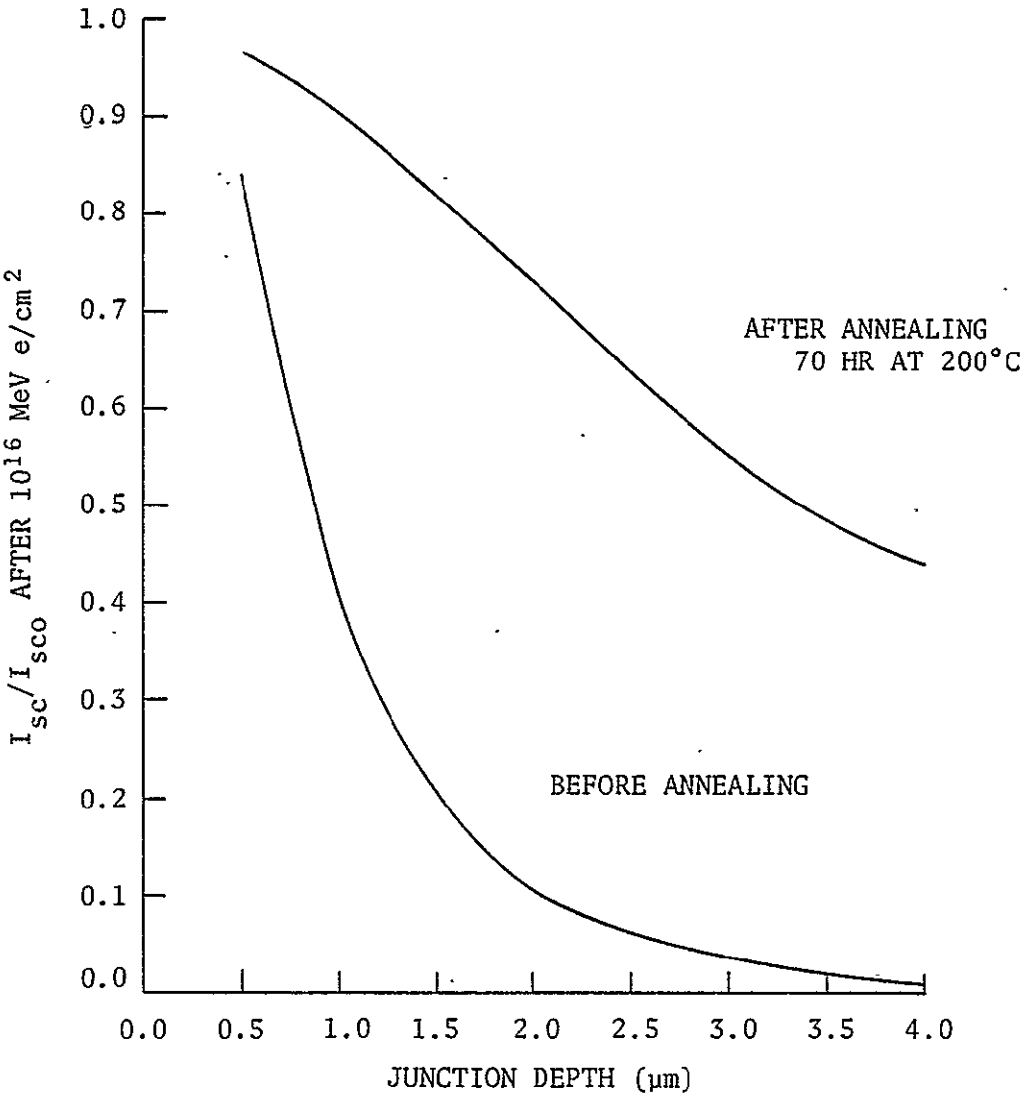

Figure 12. Annealing effects after 10^{16} 1-MeV e/cm^2 vs. junction depth (theoretical curves A = 0).

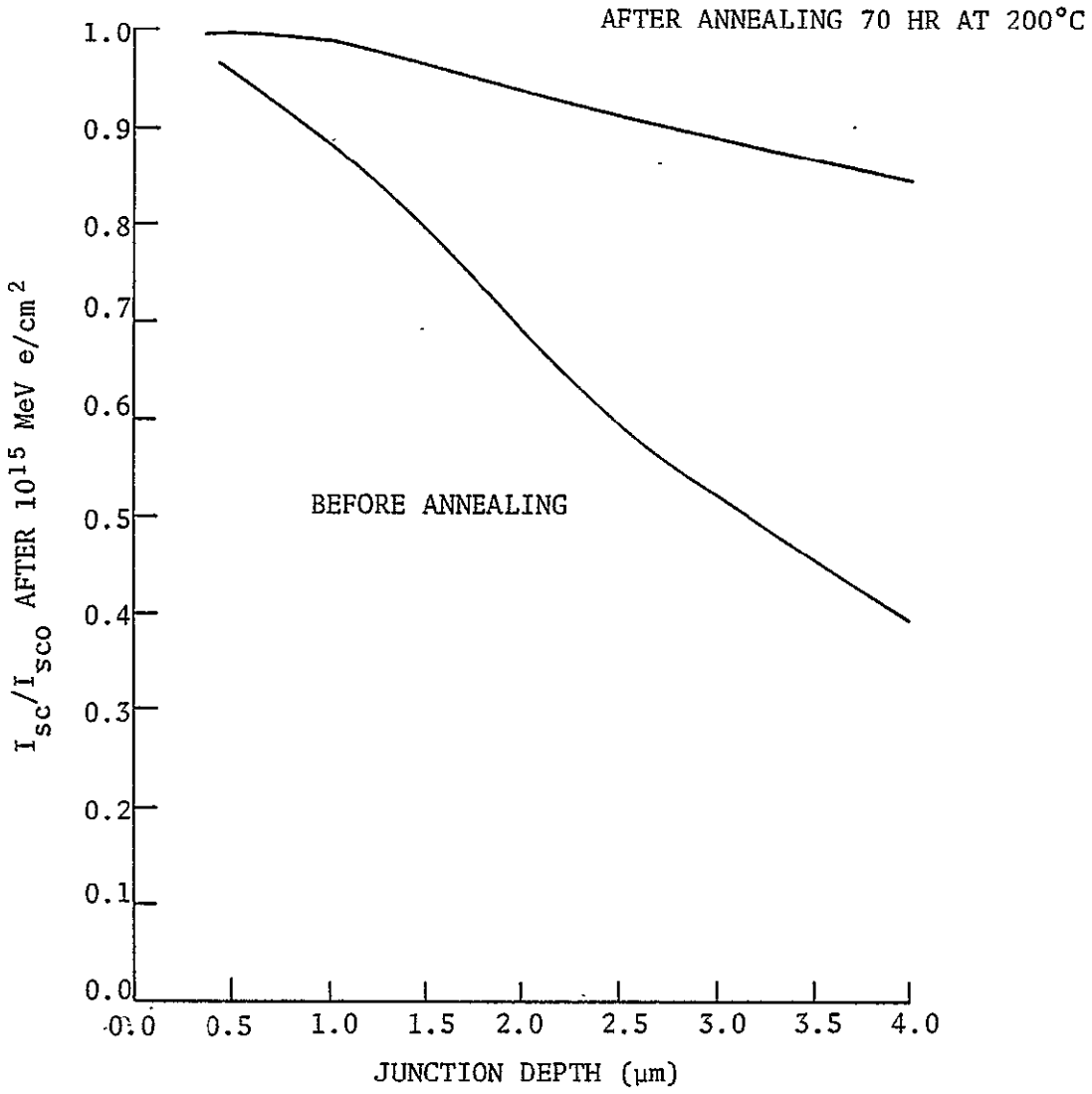

Figure 13. Annealing effects after 10^{15} 1-MeV e/cm^2 vs. junction depth (theoretical curves A = 0).

we will let $\omega_o = 0.077 \exp\{1.3/(8.6139(10^{-5})T)\}$ where T is the temperature in °K. From equation (24) we write

$$I_o = \frac{I_{sc}}{e^{x_o} - 1}$$

where $x_o = qV_{oc}/A_oKT$. Then equation (23) can be expressed as

$$I = I_{sc} - I_{sc}\left(\frac{e^{X} - 1}{e^{x_o} - 1}\right)$$

where $X = qv/A_oKT$. This equation simplifies to

$$I = I_{sc}\left\{1 - \frac{\sinh\left(\frac{X}{2}\right)}{\sinh\left(\frac{X_o}{2}\right)} e^{-(X_o - X)/2}\right\} \tag{25}$$

which is plotted in figure 14 for various values of V_{oc}/A_o.

The cell power output is given by

$$P = VI = VI_{sc}\left\{\frac{1 - \sinh\left(\frac{X_o}{2}\frac{V}{V_{oc}}\right)}{\sinh\left(\frac{X_o}{2}\right)} e^{(-X_o/2)(1 - V/V_{oc})}\right\} \tag{26}$$

where at maximum power $P = P_{max}$, $I = I_{max}$, $V = V_{max}$, and $\frac{dP}{dV} = 0$. Differentiating equation (26) we obtain that at maximum power

$$\frac{V_{oc}}{I_{sc}}\frac{I_{max}}{V_{max}} = \frac{\xi}{\sinh \xi} \exp\left\{-\xi\left(1 - 2\frac{V_{max}}{V_{oc}}\right)\right\} \tag{27}$$

where

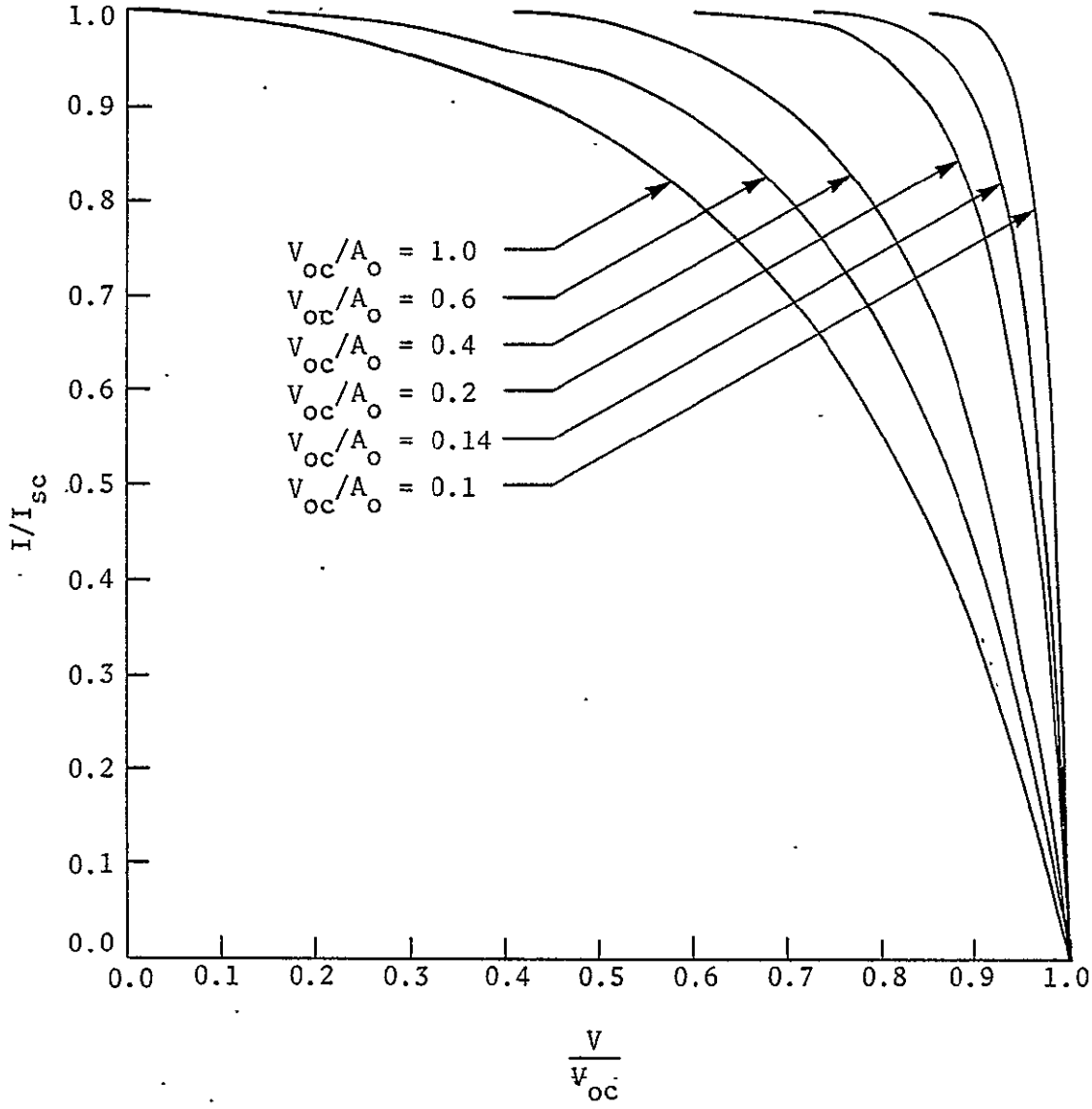

Figure 14. Current voltage curves for various values of V_{oc}/A_o.

$$\xi = \frac{X_o}{2} = \frac{qV_{oc}}{2A_o KT}$$

We may now use equation (25) to obtain the current voltage plot for irradiation for a particular cell, and we can then use equations (21) and (22) together with equation (25) to obtain after irradiation plots. These curves are illustrated in figures 15 through 18.

The theoretical curves in figures 7 through 18 agree quite well with the experimental data obtained from various annealing experiments.

Annealing During Irradiation

Consider an in situ annealing experiment where samples are irradiated with 1-MeV electrons at a rate $\tilde{\phi}$ (e/cm^2-hr) while being held at a temperature T_a (°K). We assume that production and removal of defects are a simple monomolecular process and write

$$\left\{\begin{matrix}\text{rate of change} \\ \text{of defects}\end{matrix}\right\} = \left\{\begin{matrix}\text{defects} \\ \text{produced}\end{matrix}\right\} - \left\{\begin{matrix}\text{defects removed} \\ \text{because of annealing}\end{matrix}\right\}$$

$$\frac{dN}{dt} = \sigma_d N_\ell \tilde{\phi} - \omega_o \exp\left\{-\frac{E_a}{KT_a}\right\} N \tag{28}$$

which is subject to the initial condition $N(0) = 0$.

In the case $\tilde{\phi}$ is a constant, equation (28) has the solution

$$N = \frac{\sigma_d N_\ell \tilde{\Phi}}{\omega}\left[1 - e^{-\omega\tau}\right] \tag{29}$$

where t is the anneal time and $\omega = \omega_o e^{-E_a/KT_a}$. We have that

$$\lim_{t\to\infty} N = \frac{\sigma_d N_\ell \tilde{\Phi}}{\omega}$$

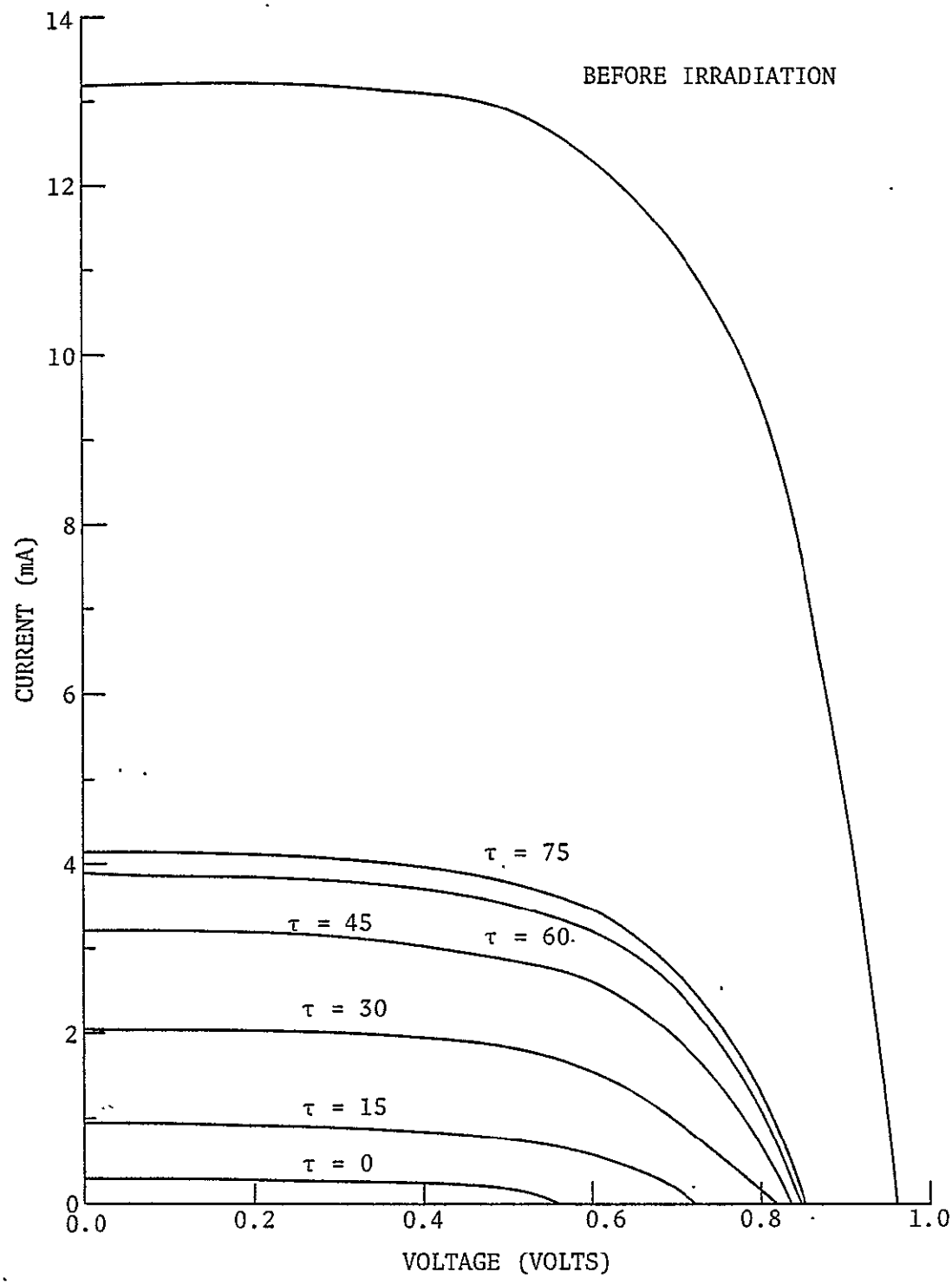

Figure 15. Current voltage characteristics of 10^{16} 1-MeV electron/cm^2 irradiated GaA/As solar cell after τ hours of annealing at 200°C obtained from statistic model.

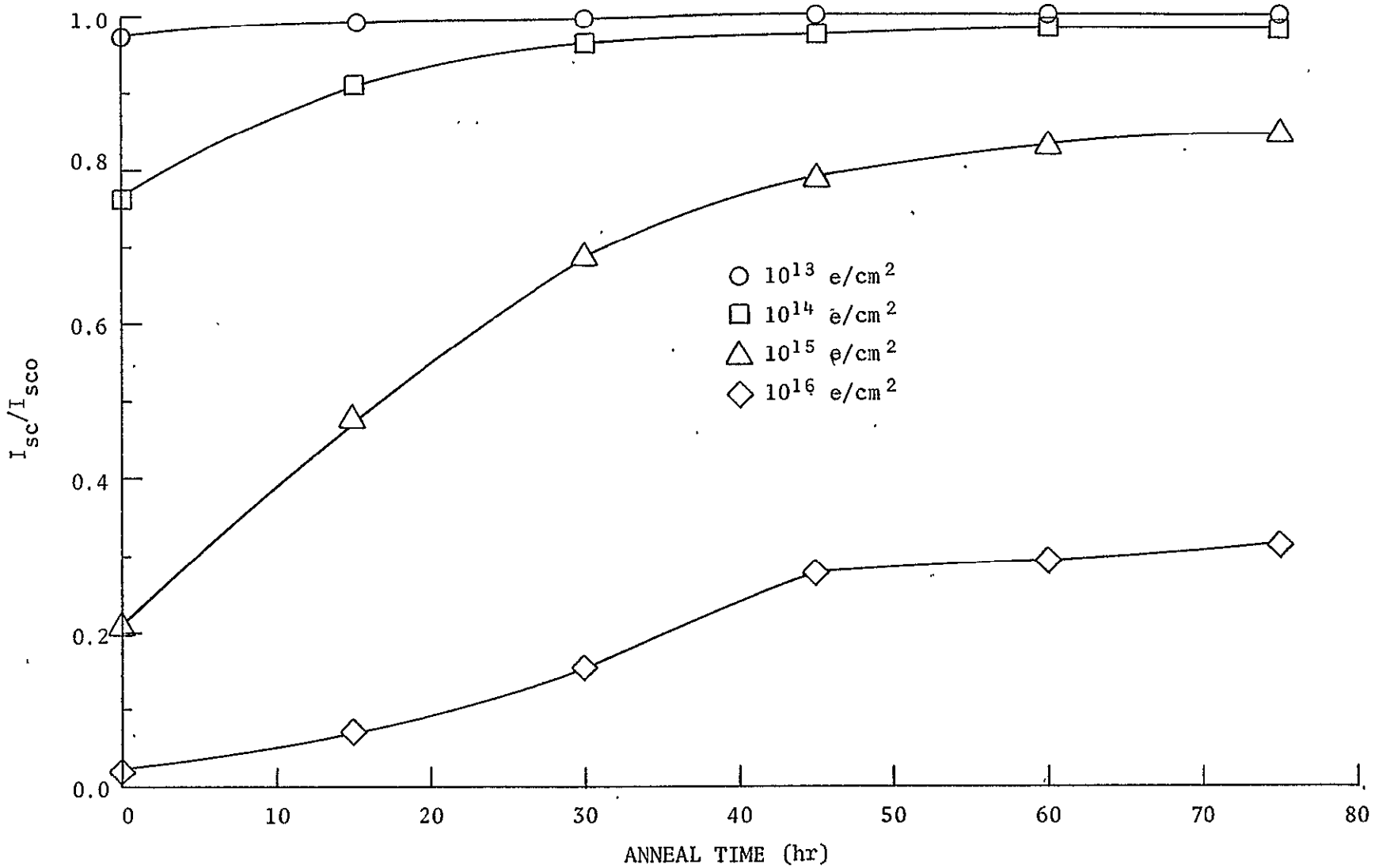

Figure 16. Short circuit current for deep junction (4-μm) cells vs. anneal time (statistical model).

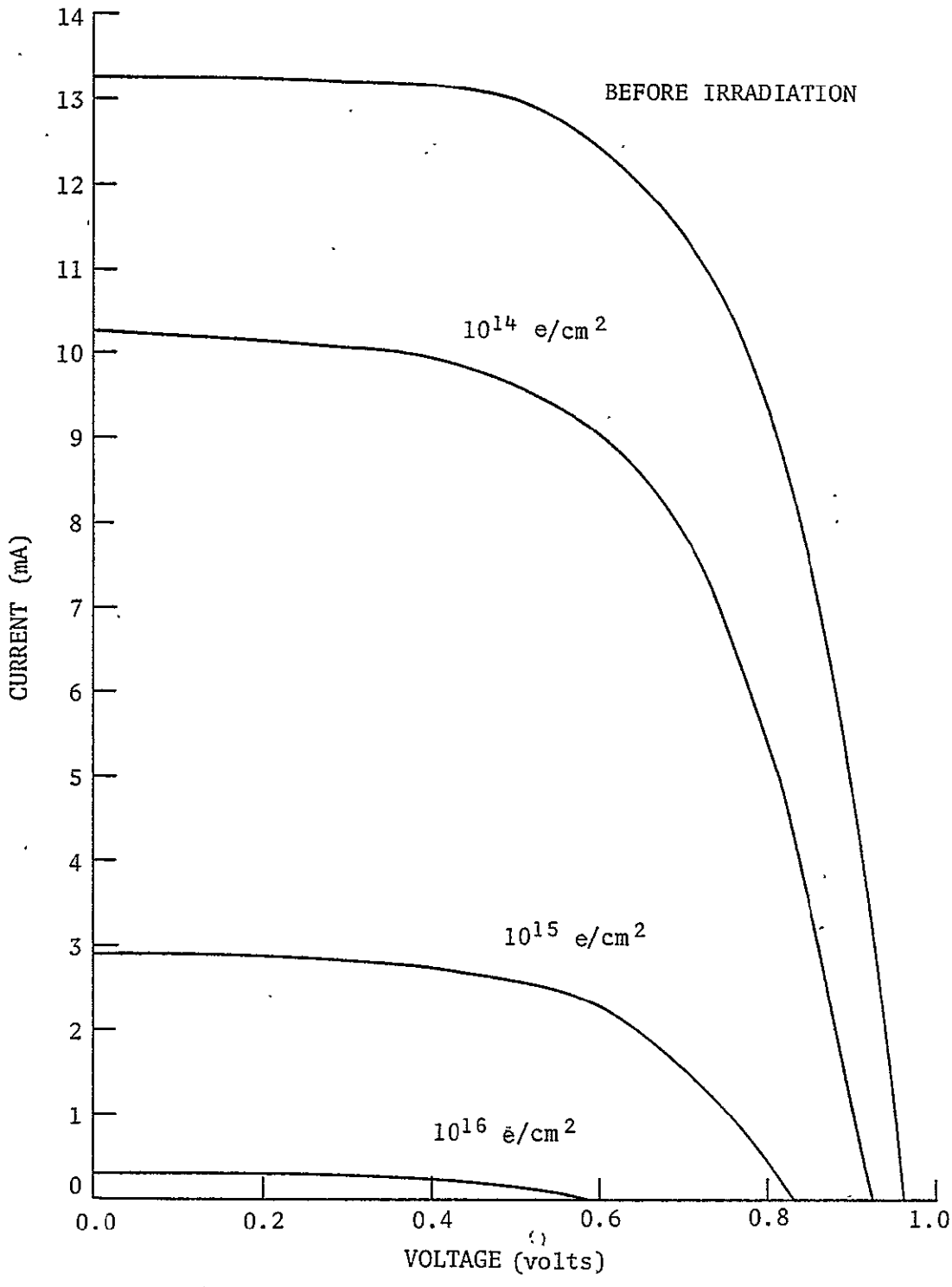

Figure 17. Current voltage curves before and after irradiation of deep junction (4-μm) cells.

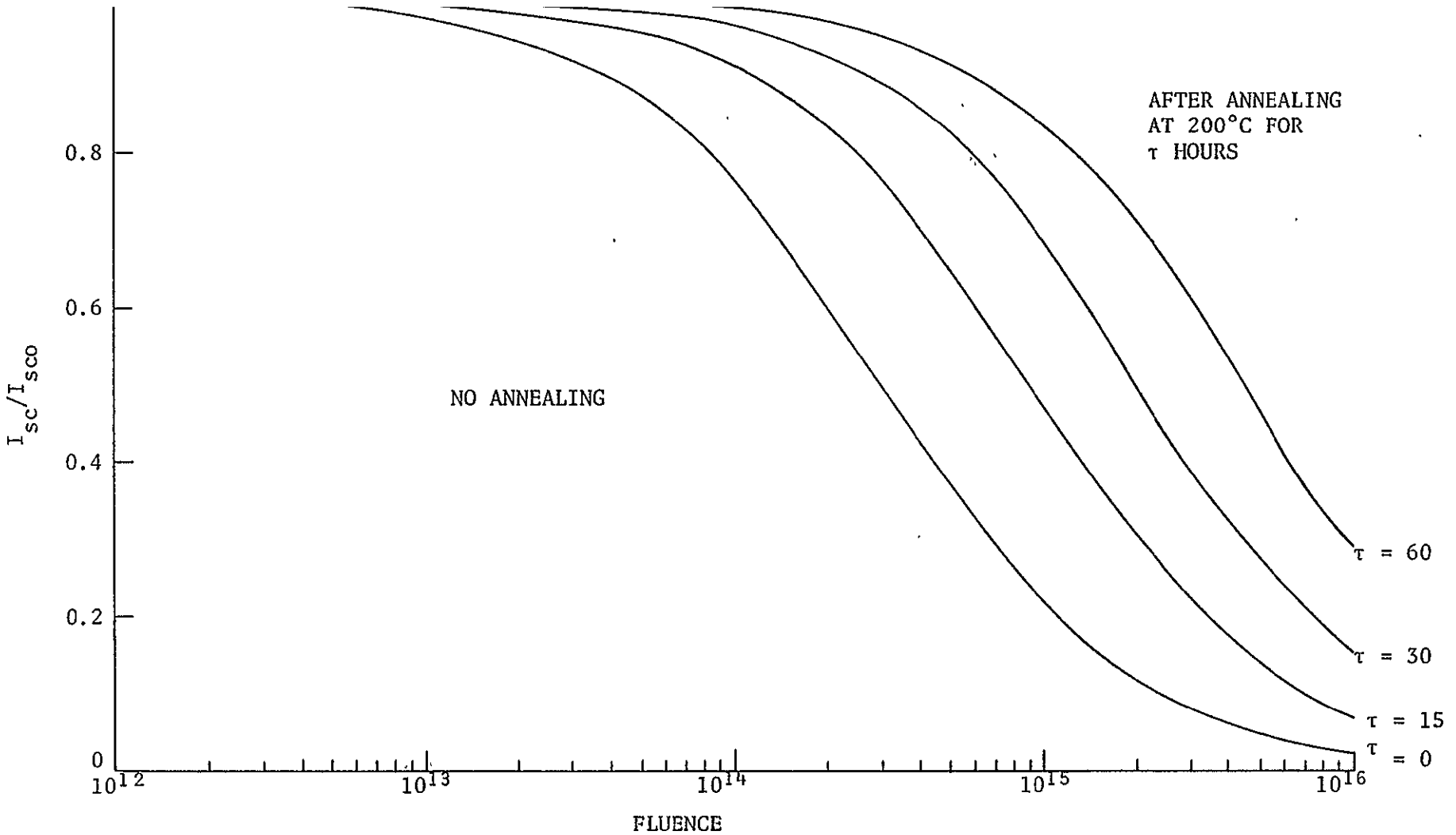

Figure 18. Annealing of deep junction (4-μm) cells as predicted by statistical model.

which says that after a long period of in situ irradiation at a constant flux rate $\tilde{\Phi}$, there will be a constant damage to the solar cell. If t is the annealing time and also the irradiation time during which the solar cell receives a fluence of ϕ (e/cm^2), then we can approximate $\tilde{\phi}$ by ϕ/t and write

$$\lim_{t\to\infty} N = \frac{\sigma_d N_\ell \Phi}{\omega t}$$

This implies that for a constant fluence Φ, the limiting damage will be smaller the longer the irradiation time t, and theoretically this limiting damage will be small after long annealing times and low dose rates.

In-Flight Experiment

During an in-flight space experiment it is assumed that the diffusion length L changes according to the relation given in equation (19), where ϕ_e is an equivalent fluence defined by

$$\phi_e = \frac{N}{\sigma_d N_\ell} \tag{30}$$

It is assumed that the defects produced are dependent upon the operating temperature T_o, the type of radiation, and the energy of the radiation. With reference to figure 19, it is assumed that the solar cells are operating at a temperature T_o over a time period $0 \leq t \leq \sigma$. During this time period, the defects produced by the irradiation increase. During the time interval $\sigma \leq t \leq \sigma + \tau$, annealing at a temperature T_a occurs which will reduce the number of defects. It is assumed that this process will be a periodic process, and we desire to study the defects produced as a function of σ, τ, T_o, and T_a.

Let

$$T = T(t) = \begin{cases} T_o, & 0 \leq t \leq \sigma \\ T_a, & \sigma \leq t \leq \sigma + \tau \end{cases} \tag{31}$$

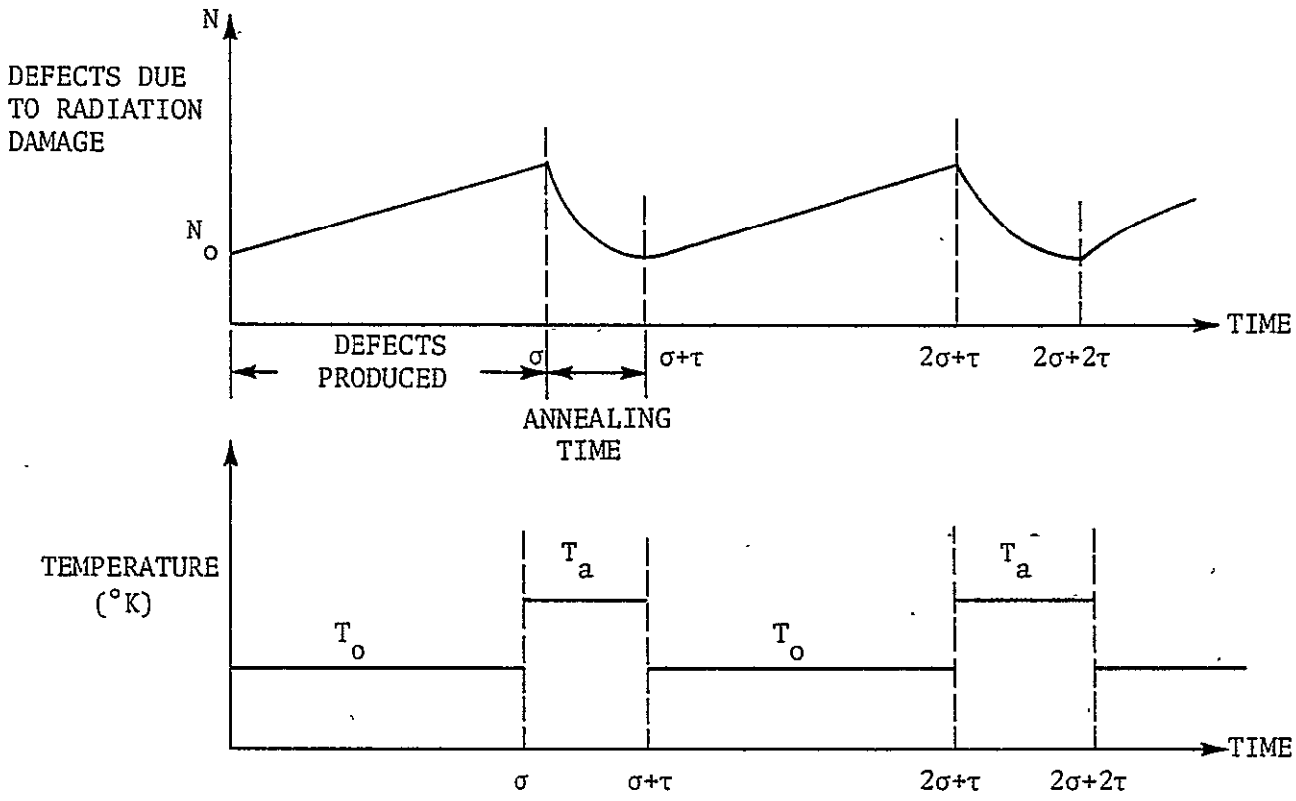

Figure 19. Radiation damage and annealing as a function of time.

with $T(t + \sigma + \tau) = T(t)$. We assume that

$$\frac{dN}{dt} = \begin{pmatrix} \text{amount} \\ \text{produced} \end{pmatrix} - \begin{pmatrix} \text{amount} \\ \text{removed} \end{pmatrix}$$

$$\frac{dN}{dt} = \phi_d N_\ell \tilde{\Phi} - \omega_o N f(t) \tag{32}$$

where

$\tilde{\Phi}$ = flux (e/cm^2-hr) (assumed constant for orbital mission)

N = number of defects/cm^3

N_ℓ = number of lattice sites/cm^3

ω_o = frequency factor

σ_d = displacement cross section

$f(t) = \exp\left\{\frac{-E_a}{KT(t)}\right\}$ = time-varying Boltzmann term where E_a is activation energy and $T(t)$ is given by equation (31).

The solution of equation (32) satisfycing $N(0) = N_o$ is given by

$$N = N(t) = \frac{1}{g(t)}\left[N_o + \sigma_d N_\ell \tilde{\Phi} \int_o^t g(s)ds\right] \tag{33}$$

where

$$g(t) = \exp\left\{\int_o^t \omega_o f(t)dt\right\} \tag{34}$$

let

$$G(t) = \exp\left\{\omega_o \int_o^t f(u)du\right\} \quad , \; 0 \leq t \leq (\sigma + \tau) = P \tag{35}$$

then, since $f(t)$ is periodic with period P, we may write

$$g(t + nP) = \exp\left\{\omega_o\, n\sigma\, e^{-\alpha} + \omega_o\, n\tau\, e^{-\beta}\right\} G(t) \tag{36}$$

where

$$\alpha = \frac{E_a}{KT_o} \qquad \text{and} \qquad \beta = \frac{E_a}{KT_a} \tag{37}$$

Then

$$N(t + nP) = \frac{1}{g(t + nP)} \left[N_o + \sigma_d N_\ell \tilde{\Phi} \int_o^{t+nP} g(s)ds\right], \quad 0 \leq t \leq P \tag{38}$$

In the limit as n increases without bound, the first term in equation (38) approaches zero, and the second term in equation (35) gives

$$\lim_{n\to\infty} \left[\frac{\int_o^{t+nP} g(s)ds}{g(t + nP)}\right] \sigma_d N_\ell \tilde{\Phi} = \frac{\sigma_d N_\ell \tilde{\Phi}}{\omega_o\, e^{-E_a/KT(t)}} \doteq N(t + nP) \tag{39}$$

Thus, after a long period of operation, the equivalent fluence is

$$\phi_e = \frac{\tilde{\Phi}}{\omega_o \exp\{-E_a/KT(t)\}}$$

which varies between the minimum value of

$$\phi_{e,min} = \frac{\tilde{\Phi}}{\omega_o e^{-\alpha}}$$

and maximum value of

$$\phi_{e,max} = \frac{\tilde{\Phi}}{\omega_o e^{-\beta}}$$

where ω_o is the frequency factor. The resulting damage to the diffusion length varies between L_{min}, determined by

$$\frac{1}{L_{min}^2} = \frac{1}{L_o^2} + K_g \Phi_{e,min}$$

and L_{max}, determined by

$$\frac{1}{L_{max}^2} = \frac{1}{L_o^2} + K_g \Phi_{e,max}$$

If the junction depth X_j is such that $X_j < L_{min} < L_{max}$, then there will be no observable damage to the electrical characteristics, as any minority carriers produced by photon impingement will be guaranteed arriving at the junction.

CONCLUSIONS

In this report we studied heteroface GaAlAs-GaAs solar cell operation in the temperature range 25° to 350° C. The striking difference between our work and previous reports is that we raised the operating temperature beyond 250° C. We looked into illuminated light J-V, dark J-V curves, and comprehensive spectral response characteristics as a function of temperature. From the illuminated light current voltage curves, the slopes $\Delta V/\Delta T$, $\Delta J/\Delta T$, $\Delta FF/\Delta T$, and $\Delta \eta/\Delta T$ were measured and compared with previous reports.

The actual measurement of efficiency near 350° C was observed to be approximately 2 percent at AMO, which is somewhat lower than the extrapolated values obtained from other sources. From the dark current voltage measurements, we observed that the A-factor value decreases from A = 2.1 to A = 1.5 with increasing temperature (up to 350° C). Assuming that A = 2 for all temperatures, we could calculate the composite recombination lifetime as a function of temperature. The difficulty in defining the slope of the ln(J) - V curve forced us to assume that A = 2 in order to obtain the recombination lifetime. Consequently, we could only obtain a crude

approximation for the lifetime using this technique. The recombination lifetime was also obtained from the spectral response measurements. The resulting values of the recombination lifetimes obtained by these two methods gave results which differed by a factor of 10. It is believed that the discrepancy between the values calculated by these two methods was due to the crude approximation in defining the A-value slope in the dark current voltage curves.

We also obtained a comprehensive spectral response characteristic as a function of temperature. The values of the spectral response were obtained both theoretically and experimentally. In order to calculate the theoretical spectral response curves, the absorption coefficients of AlGaAs were modeled to change with temperature in a manner which agreed with the band gap change with temperature. A computer fit of experimental and calculated spectral response data produced many photovoltaic parameters as a function of temperature. We found that the aluminum content, the recombination velocity at the AlGaAs-pGaAs interface, the diffusion length in pGaAs, and the lifetime in pGaAs were critical parameters which help determine the spectral response at the blue end of the spectrum. The parameters in the nGaAs layer which determine the spectral response in the red end of the spectrum were found to be the diffusion length, diffusion coefficient, and lifetime.

Annealing models were constructed assuming both monomolecular and bimolecular reactions for the interstitial-vacancy recombination reactions. These theoretical models produced curves which agree quite well with the experimental data.

REFERENCES

1. Kalma, A.H.; and Berger, R.A.: Electrical Properties of Electron-Irradiation GaAs. IEEE Trans. Nuclear Science, Vol. NS-19, No. 209, 1972.

2. Lang, D.V.; Logan, R.A.; and Kimerling, L.C.: Identification of the Defect State Associated with a Gallium Vacancy in GaAs and $Al_xGa_{1-x}As$. Physics Review, Vol. B15, No. 4874, 1977.

3. Walker, G.H.; and Conway, E.J.: Short Circuit Current Changes in Electron Irradiated GaAlAs/GaAs Solar Cells. IEEE PhotoVoltaic Specialist Conference, Vol. 13, No. 575, 1978.

4. Goldstein, B.: Diffusion in Compound Semi-Conductors. Physics Review, Vol. 121, No. 1305, 1961.

5. Casey, H.C., Jr.; and Panish, M.B.: Reproducible Diffusion of Zinc into GaAs: Application of the Ternary Phase Diagram and the Diffusion and Solubility Analyses. Transactions of the Metalurgical Soc. of AIME, Vol. 242, No. 406, 1968.

6. Chang, L.L.: The Junction Depth of Concentration-Dependent Diffusion of Zinc in III-V Compounds. Solid State Electronics, Vol. 7, No. 853, 1964.

7. Chang, L.L.; and Koma, A.: Interdiffusion Between GaAs and AlAs. Appl. Phys. Letters, Vol. 29, No. 138, 1976.

8. Lou, C.Y.; and Somorjsi, G.A.: Studies of the Vaporization Mechanism of Gallium Arsenide Single Crystals. J. Chem. and Phys., Vol. 55, No. 4554, 1971.

9. Arthur, J.R.: Surface Stoichiometry and Structure of GaAs. Surface Science, Vol. 43, No. 449, 1974.

10. Sebestyen, T.; Menyhard, M.; and Szigethy, D.: In Situ Measurements of Arsenic Losses During Annealing of the Usual Evaporated Contacts of GaAs Gunn Diodes. Electronics Letters, Vol. 12, No. 96, 1976.

11. Hovel, H.; and Woodall, J.M.: Optimization of Solar Cells for Air Mass Zero Operation and a Study of Solar Cells at High Temperatures. NASA CR-145268, 1976.

12. Goldhammer, L.J.; Knechtti, R.; Kamath, S.; and Loo, R.: High Energy Proton Radiation Damage to AlGaAs-GaAs Solar Cells." Rockwell International Contractor Report, 1977.

13. Hovel, H.: Semiconductors and Semimetals. II: Solar Cells. Academic Press (NY), 1975.

14. Stirn, R.J.: Junction Characteristics of Silicon Solar Cells. Proc. 9th IEEE Photovoltaic Specialist Conference, p. 72, 1972.

15. Heinbockel, J.H.; and Doviak, M.J.: Long-Term Radiation Effects on GaAs Solar Cell Characteristics. Final Report, NASA Grant NSG 1426, May 31, 1978.

16. Chafin, R.J.: Microwave Semiconductor Devices: Fundamental and Radiation Effects. John Wiley and Sons (NY), 1973.

17. Dienes, G.J.; and Vineyard, G.A.: Radiation Effects in Solids. Interscience Publishers, Inc. (NY), 1957.

18. Kelly, B.T.: Irradiation Damage to Solids. Pergamon Press (NY), 1966.

19. Spitsyn, A.V.; and Smirnov, L.S.: Theory of the Annihilation of Radiation Defects in Semiconductors. Soviet Physics - Solid State, Vol. 4, No. 12, June 1963.

20. Potts, H.R.; and Pearson, G.L.: Annealing and Arsenic Overpressure Experiments on Defects in Gallium Arsenide. J. Appl. Phys., Vol. 37, No. 5, Apr. 1966.